ENHANCED SCATTERING OF LASER LIGHT BY OPTICAL MIXING IN A PLASMA

by

BARRY LIONEL STANSFIELD
B.A.Sc., University of Toronto, 1965
M.A.Sc., University of British Columbia, 1967

A THESIS SUBMITTED IN PARTIAL FULFILMENT OF
THE REQUIREMENTS FOR THE DEGREE OF
DOCTOR OF PHILOSOPHY

in the Department
of
PHYSICS

We accept this thesis as conforming to the
required standard

THE UNIVERSITY OF BRITISH COLUMBIA
February, 1971

In presenting this thesis in partial fulfilment of the requirements for an advanced degree at the University of British Columbia, I agree that the Library shall make it freely available for reference and study. I further agree that permission for extensive copying of this thesis for scholarly purposes may be granted by the Head of my Department or by his representatives. It is understood that copying or publication of this thesis for financial gain shall not be allowed without my written permission.

Department of Physics

The University of British Columbia
Vancouver 8, Canada

Date April 28th, 1971

ABSTRACT

The enhancement of the scattered light signal due to the mixing of two optical beams in a plasma has been observed. The two beams are produced in a dual-cavity organic dye laser pumped by a Q-switched ruby laser. The plasma is generated by a Helium plasma jet. In normal scattering a distinct satellite is observed on either side of the incident ruby wavelength 6943Å. The presence of enhanced oscillations is demonstrated by a significant increase in the intensity of one of these satellites when the dye lasers are tuned such that the difference in their frequencies is equal to the normally-observed resonant frequency of the plasma.

TABLE OF CONTENTS

LIST OF TABLES

LIST OF ILLUSTRATIONS

ACKNOWLEDGEMENTS

I would like to thank Dr. R. Nodwell for his enthusiastic support and timely suggestions during the course of the experiment. I would also like to thank Dr. J. Meyer for valuable help during Dr. Nodwell's leave, and Dr. T. S. Brown and Dr. L. Sobrino for helpful discussions.

I would like also to acknowledge the work of the technical staff in construction of some of the equipment. Special thanks are also extended to the members of the Plasma Physics group whose friendship and help were invaluable, in particular Mr. H. Baldis, Mr. M. Churchland and Mr. R. Morris.

Financial assistance from National Research Council, B. C. Hydro and U.B.C. fellowships is gratefully acknowledged.

This work is supported by a grant from the Atomic Energy Control Board of Canada.

CHAPTER I

INTRODUCTION

With the invention of the giant-pulse ruby laser, light scattering has become a practical technique for the study of laboratory plasmas. It has the advantage of very good temporal and spatial resolution, while at the same time disturbing the plasma very little if at all. A major difficulty with the technique is that the Thomson cross-section σ_T is very small so that usually only about 10^{-12} of the incident light is scattered into the detector. With such a small signal the problems of stray light can be severe, especially if the plasma is contained within a vacuum vessel of any kind. As long as one scatters only from thermal fluctuations one cannot hope to improve on the signal strength since the average cross-section per electron is close to σ_T.

There have been several cases in which an enhanced scattering due to nonthermal fluctuations of a plasma have been observed, but these have depended on unusual conditions in the plasma itself, and so cannot be considered a generally applicable diagnostic tool. In ionospheric backscatter the plasma satellites were greatly enhanced by the

presence of suprathermal electrons produced by the action of solar ultra-violet light (see Perkins, Salpeter and Yngvesson (1965) and Perkins and Salpeter (1965)). Similar large enhancements have been observed when scattering from collisionless shock waves (see Daughney, Holmes and Paul (1970)).

A plasma is not a linear medium; it responds nonlinearly to an electromagnetic field impressed upon it. These nonlinearities have been receiving more attention in recent years, as is shown by the recent publications of several books devoted to nonlinear plasma theory: Kalman and Feix (1969), Sagdeev and Galeev (1969) and Tsytovich (1970).

Methods have been proposed by Berk (1964) and Kroll, Ron and Rostoker (1964) for making use of the plasma nonlinearity in scattering experiments. The process suggested by Berk consists of driving plasma oscillations with an electromagnetic wave with frequency close to, but slightly higher than, the plasma frequency. This technique is limited to plasmas with electron densities less than about 10^{14} cm^{-3} since microwave generators are the only convenient tunable source whose frequency can approach the plasma frequency. In the future, parametric converters operating in the infrared may prove to be useful in extending this technique to higher densities. The scheme suggested by

Kroll, Ron and Rostoker doesn't suffer from this disadvantage, since it predicts that plasma oscillations can be generated by two electromagnetic waves incident on the plasma, the frequency difference between them being close to the plasma frequency. This does require, however, that we produce two powerful beams which can be tuned to a given frequency difference. The development, in the last few years, of the organic dye laser has made this possibility a reality. By pumping an organic dye with a giant-pulse laser it is possible to produce powerful pulses (containing up to 25% of the energy of the pump) of radiation, the wavelength of emission being tunable over the fluorescence band of the molecule.

Such a dye laser is used in our investigation, in a novel configuration, to produce the two beams required in the mixing experiment. The wavelength difference can be varied over about 80Å, sufficient to resonate with most plasmas. The power output and the linewidth of the laser are sufficient to allow us to generate plasma waves in the Helium plasma produced by a plasma jet. Enhanced scattering is observed when the frequency difference between the two dye laser beams is tuned to the normally-observed plasma resonance.

Chapter II of the thesis is a summary of the theory for scattering from a plasma, and a derivation of the

generation of plasma waves by nonlinear interactions in a plasma. Chapter III contains a description of the experiment, and the results are given in Chapter IV. Chapter V contains a summary of the results obtained, as well as a discussion of some possible new experiments.

Appendix A has been added as a summary of earlier work done to develop a Raman laser as the source of the mixing beams. Appendix B is a brief analysis of the damping processes which limit the resonance and hence determine the size of the enhanced fluctuation.

CHAPTER II

THEORY

A. SUMMARY OF SCATTERING THEORY

The theory of laser scattering from a plasma has been derived by several authors, and is well summarized by Bekefi (1966), Chan (1966), and Evans and Katzenstein (1969). The process is considered classically in the following stages: an electromagnetic wave incident on the plasma causes the electrons to be accelerated, these accelerated electrons then radiate, the electric vector from a large number of these electrons being summed to obtain the resultant electric field vector for the ensemble.

The signal associated with this resultant field will be significant only when there is some non-uniformity in the distribution of the charges. These spatial inhomogeneities may be microscopic or macroscopic, the microscopic variations being a direct result of the particle nature of the electrons whereas the macroscopic variations are a result of fluctuations in the smeared-out fluid plasma.

If a plane monochratic electromagnetic wave of frequency w_o and flux density F_i in the direction $\underline{k}_o$ is incident on the plasma of volume V_s, as shown in fig. 2-1,

then the scattered power in a solid angle $d\Omega$ about the direction $\underline{k}$, and in the frequency interval dw about w is given by:

$$P_s(\underline{k},w)\ dwd\Omega = \frac{r_0^2}{2\pi}\ (1-\cos^2\theta)\ n_e\ V_s\ F_i\ \ s(\underline{\Delta k},\Delta w)\ dwd\Omega$$

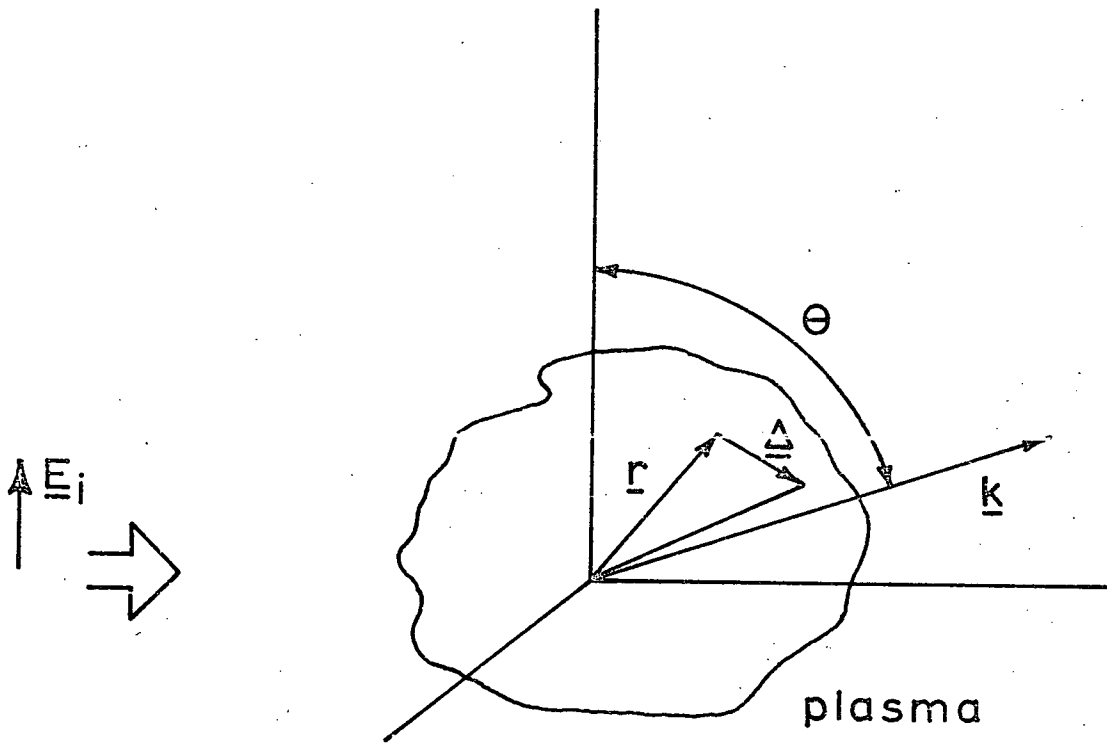

Fig. 2-1

SCATTERING OF RADIATION FROM A PLASMA

where: r_o is the classical radius of the electron

θ is the scattering angle measured from the direction of the incident electric field $\underline{E}_i$

n_e is the electron number density

and

$S(\underline{\Delta k}, \Delta w)$ is the spectral density of electron density fluctuations.

Thus, in a scattering experiment we directly measure the Fourier spectrum of the electron density fluctuations in the plasma. The spectral density can be expressed in two forms:

$$S(\underline{\Delta k}, \Delta w) = \mathcal{F}\left[C_n(\Delta, \tau)\right]$$

$$= \lim_{Vs,\, T\to\infty} \frac{2}{VsT} \frac{|n_e(\underline{\Delta k} = \underline{k}-\underline{k}_0,\ \Delta w = w-w_0)|^2}{n_e}$$

Here $C_n(\underline{\Delta},\tau)$ denotes the space-time autocorrelation function of the electron density:

$$C_n(\underline{\Delta},\tau) \equiv \frac{1}{Vs} \int_{Vs} d\underline{r}\, \frac{1}{T} \int_{-T/2}^{T/2} dt\ \ n_e(\underline{r},t)\ n_e(\underline{r}+\underline{\Delta},\ t+\tau)$$

and $\mathbb{F}$ denotes the Fourier transform centered on $\underline{k}_o, w_o$:

$$\int d\underline{r}\, dt\, n_e(\underline{r},t)\, e^{-i[(w-w_o)t-(\underline{k}-\underline{k}_o)\cdot\underline{r}]}$$

$$\equiv \mathbb{F}\left(n_e(\underline{r},t)\right)$$

We find the first expression to be more useful in calculating the scattering from a macroscopic wave.

Calculations of $S(\Delta\underline{k}, \Delta w)$ for an almost-Maxwellian plaxma yield a scattered spectrum whose shape is determined by the correlation parameter $\alpha = \frac{1}{\Delta k L_D}$, where Δk is the magnitude of the scattering wavevector and L_D is the plasma Debye length. For $\alpha>1$, the wavelength of the fluctuations which give rise to scattering in the direction $\underline{k}$ is longer than the Debye length. In this case we might expect to observe some features due to long-range correlations, and in fact calculations and experiment (see Chan and Nodwell (1966), Ramsden and Davies (1966)) confirm the presence of satellites symmetrically displaced from the incident frequency by about the plasma frequency.

Thus observation of these satellites, and measurement of the frequency shift should give direct information about the plasma density.

B. ESTIMATION OF THE SIGNAL-SCATTERING FROM A THERMAL PLASMA

There are two reasons for calculating the scattered signal:

(i) to see what size of signal we receive, and so provide a yardstick against which we can estimate the feasibility of measuring the enhanced oscillations;

(ii) to estimate the problems of a small signal superimposed on noise. The noise may be due to the inherent fluctuations (shot noise) of either the scattered signal itself, or the light from the plasma.

The power scattered into a solid angle $d\Omega$ in a frequency interval dw is:

$$dPs = N F_i \frac{r_0^2}{2\pi} (1-\cos^2\theta) S(\underline{\Delta k}, \Delta w) d\Omega dw$$

where: $N = n_e Vs$ is the total number of scattering, particles in the scattering volume Vs, which is assumed to be a cube of linear dimension $\ell = 300\mu$.

In terms of the numbers of photons, we have:

$$F_i = \frac{P_i}{A} = \frac{n_i h\nu}{\tau A}$$

and

$$dP_s = \frac{n_s h\nu}{\tau}$$

where: n_i and n_s are the numbers of incident and scattered photons of frequency ν, and τ is the duration of the laser pulse, and A is the area of the beam. Hence we have:

$$\frac{n_s}{n_i} = n_e \ell \frac{r_o^2}{2\pi} (1-\cos^2\theta)\, S(\underline{\Delta k}, \Delta w)\, d\Omega dw$$

From the theoretical calculations, which are shown in fig. 2-2, we have for a Helium plasma with T_e = 17000K and $n_e = 2.2 \times 10^{16}$ cm^{-3} an average value of $S(\underline{\Delta k}, \Delta w) = 1.3 \times 10^{-13}$ over a 3Å wide band centered on the satellite.

For a reasonably good collecting system of f/6 we have $d\Omega \simeq 2\times10^{-2}$ Sr. The 3Å band corresponds to a frequency band $dw \simeq 1.2\times10^{12}$ sec^{-1}. Using these values we obtain:

$$\frac{n_s}{n_i} \simeq 1.27 \times 10^{-14} .$$

What size of signal would be expected from this sort of scattering ratio? In a 100 mj ruby laser pulse there are about 3×10^{17} photons, so if we assume this many enter the focal spot, we have $n_s \simeq 3.8\times10^{3}$ photons. If our photomultiplier has a 3% quantum efficiency near 6943Å (typical of an S-20 photocathode) then we have about 115 photoelectrons produced. With a gain of 10^7 (approximate value for an R.C.A. 7265 tube at 2400V.) and a pulse width of 40 nanosec., we have an anode current of $i_a \simeq 4.6\times10^{-3}$ amps. Across a 25Ω load this current gives a voltage of 115 mV.

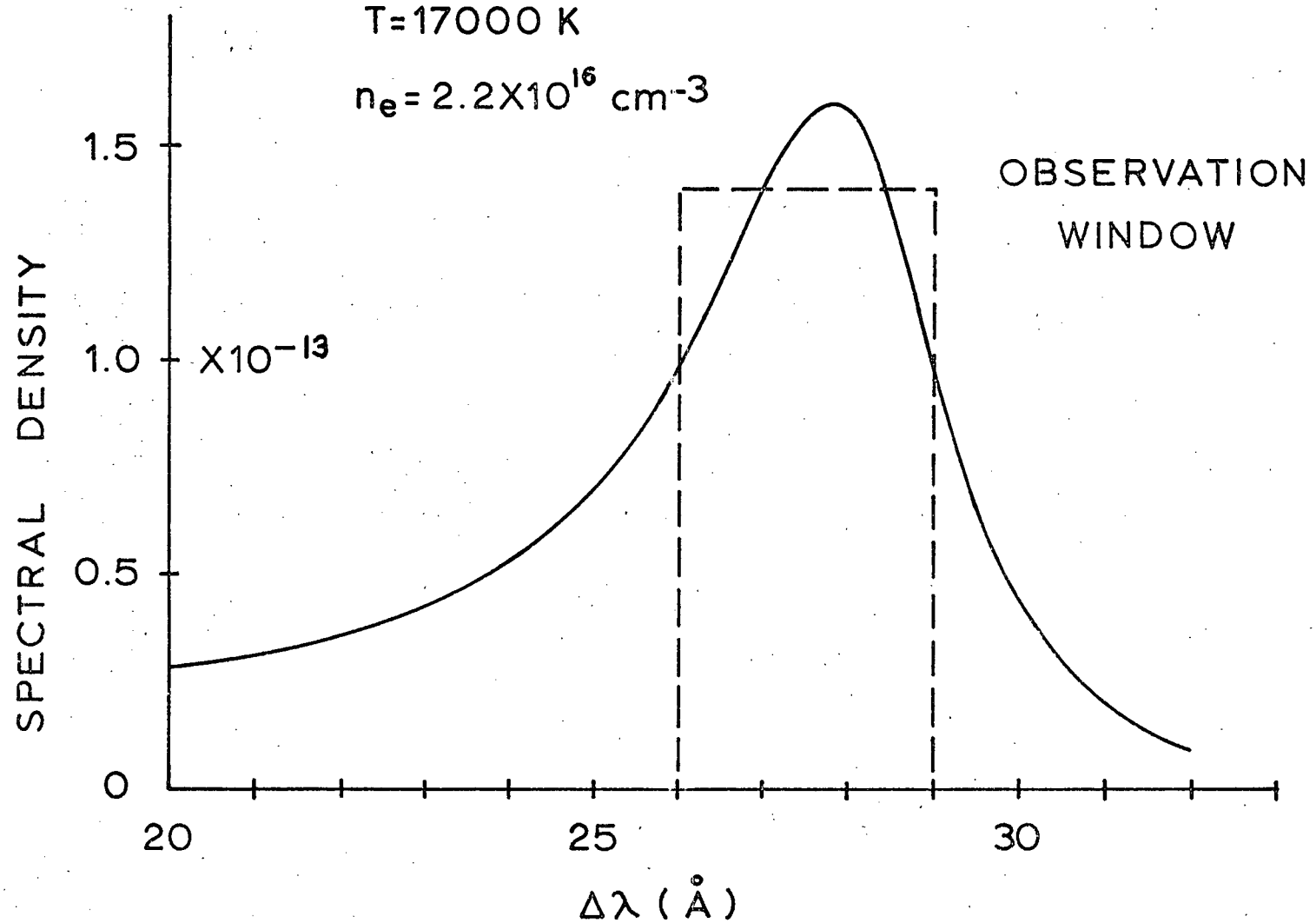

Fig. 2-2

THEORETICAL SCATTERED SPECTRUM FOR HELIUM PLASMA WITH $n_e = 2.2x10^{16}$ cm^{-3}, T_e = 17,000 K.

This is approximately (within a factor of 3) the value of the voltage spike observed when scattering near the satellite frequency. As we can see, this signal is derived from only a small fraction of the photons which enter the focal spot.

Under ideal circumstances this signal should be easily detected, and the noise in the case of a perfectly reproducible plasma would be the shot noise of the scattered photons, the $\left(S/N\right)$ ratio detected being degraded by the low quantum efficiency (see Arcese (1964)):

$$\left(\frac{S}{N}\right)_{\text{detected}} \simeq \sqrt{n_s \eta} \simeq 10 \ ,$$

where η is the quantum efficiency of the photocathode.

When we observe the light scattered from a luminous plasma, the scattered signal will be superimposed on a noisy background. The emission from the plasma can be due to free-free (bremsstrahlung) or free-bound (radiative recombination) transitions. The free-free radiation can be expressed by an emission coefficient (see Bekefi (1966) p. 89):

$$jw = 2.39 \times 10^{-53} \frac{n_e n_i}{T_e^{\frac{1}{2}}} \left[\frac{\pi G}{\sqrt{3}}\right] \frac{\text{Watts}}{(\text{radian. Sr.m}^3)}$$

The Gaunt factor $\frac{G}{\sqrt{3}} \simeq 2$ for radiation in the optical region of the spectrum. For the plasma considered here, the free-free emission coefficient can be expressed:

$$jw \simeq 6.22 \times 10^{8} \frac{\text{Photons}}{\text{radian.Sr.m}^3\text{.sec.}}$$

so from the volume Vs the number of photons collected is $\simeq 20$.

The ratio of the free-bound to the free-free radiation can be estimated (see Zel'dovich and Raizer (1966) p. 272) to be:

$\frac{f\text{-}b}{f\text{-}f} \simeq \frac{e^{h\nu/kT}-1}{1}$, where ν is

the frequency of the emitted photon. For a ruby-wavelength photon, and T ≃ 17,000 K, we find:

$$\frac{f-b}{f-f} \simeq 2 ,$$

so that the total number of collected noise photons is ≃ 60. Since only about 2 of these are detected, we see that for the Helium jet the shot noise of the scattered photons is the dominant noise source.

C. WAVE-MIXING - GENERATION OF A LONGITUDINAL WAVE

The original calculation of the generation of a density wave by wave-mixing was made by Kroll, Ron and Rostoker (1964). Their result can be derived in a simple manner, including the correction to the resonance profile pointed out by Shkarofsky (1966, 1968). The procedure consists in calculating the velocity of the electrons when accelerated by the electric field of the incident wave, and their subsequent acceleration in the magnetic field of the wave. The Lorentz force is then inserted into the Vlasov equation to calculate the density fluctuation.

It should be noted that the calculation does not incorporate the normal incoherent scattering results but, as pointed out by Weinstock (1967), the coherent and incoherent scattering are additive and hence can be calculated separately.

We assume that the incident wave is composed of two plane, monochromatic waves:

$$E(\underline{r},t) = \underline{E}_1 \cos(w_1 t - \underline{k}_1 \cdot \underline{r})$$

$$+ \underline{E}_2 \cos(w_2 t - \underline{k}_2 \cdot \underline{r})$$

To a first approximation the perturbation of the electon's velocity is only due to the acceleration in the electric field:

$$\dot{\underline{v}}_1 = \frac{e}{m}\left[\underline{E}_1(\underline{r},t) + \underline{E}_2(\underline{r},t)\right]$$

Upon integration this gives:

$$\underline{v}_1 = \frac{e}{m}\left[\underline{E}_1 \frac{\sin(w_1 t - \underline{k}_1 \cdot \underline{r})}{w_1}\right.$$

$$\left. + \underline{E}_2 \frac{\sin(w_2 t - \underline{k}_2 \cdot \underline{r})}{w_2}\right]$$

Now we consider the nonlinear second-order force on the electron due to the Lorentz force. Since the electron has attained a velocity $\underline{v}_1$ from being accelerated by the electric field, it experiences a force:

$$m\dot{\underline{v}}_2 = e \frac{\underline{v}_1 \times \underline{B}}{C}$$

which arises from the interaction with the magnetic field of the wave:

$$B(\underline{r},t) = \underline{B}_1(\underline{r},t) + \underline{B}_2(\underline{r},t)$$

$$= \frac{\underline{k}_1 x \underline{E}_1(\underline{r},t)}{k_1} + \frac{\underline{k}_2 x \underline{E}_2(\underline{r},t)}{k_2}$$

Hence the acceleration produced at $(\underline{r},t)$ is:

$$\dot{\underline{v}}_2 = \frac{e}{m} \frac{\underline{v}_1 \times \underline{B}(\underline{r},t)}{C}$$

$$= \frac{e^2}{m^2 c} \left[\underline{E}_1 \frac{\sin(w_1 t - \underline{k}_1 \cdot \underline{r})}{w_1} + \underline{E}_2 \frac{\sin(w_2 t - k_2 r)}{w_2} \right]$$

$$x \left[\frac{\underline{k}_1 \times \underline{E}_1}{k_1} \cos(w_1 t - \underline{k}_1 \underline{r}) + \frac{\underline{k}_2 \times \underline{E}_2}{k_2} \cos(w_2 t - k_2 r) \right]$$

We see that the vector product will give rise to four terms, which we consider in pairs:

(a) $\underline{E}_1 \times (\underline{k}_1 \times \underline{E}_1) = \underline{k}_1 (\underline{E}_1 \cdot \underline{E}_1)$

and

$\underline{E}_2 \times (\underline{k}_2 \times \underline{E}_2) = \underline{k}_2 (\underline{E}_2 \cdot \underline{E}_2)$

produce accelerations along $\underline{k}_1$ at frequencies 2w, and zero, and along $\underline{k}_2$ at frequencies $2w_2$ and zero. At high frequency the acceleration cannot produce any spatial density fluctuation since the particles can have very little displacement in the time available. The DC terms give rise to the classical analogue of Compton momentum transfer.

(b) $$\underline{E}_1 \times (\underline{k}_2 \times \underline{E}_2) = \underline{k}_2(\underline{E}_1 \cdot \underline{E}_2) - \underline{E}_2(\underline{E}_1 \cdot \underline{k}_2)$$

$$\underline{E}_2 \times (\underline{k}_1 \times \underline{E}_1) = \underline{k}_1(\underline{E}_1 \cdot \underline{E}_2) - \underline{E}_1(\underline{k}_1 \cdot \underline{E}_2)$$

At this point assume that $\underline{E}_1$ and $\underline{E}_2$ are parallel, and are perpendicular to the plane formed by $\underline{k}_1$ and $\underline{k}_2$ (which is the experimental situation).

We are then left with $\underline{k}_2(\underline{E}_1 \cdot \underline{E}_2)$ and $\underline{k}_1(\underline{E}_1 \cdot \underline{E}_2)$, which contain accelerations along $\underline{k}_2$ and $\underline{k}_1$ at the sum and difference frequencies. Again, since $w_1 + w_2$ is a high frequency, the electrons have no time to respond to the sum-frequency acceleration. The difference frequency can be made arbitrarily small, and hence can move the electrons over macroscopic distances and hence could produce density fluctuations.

If we only retain the difference-frequency terms, we have:

$$\dot{\underline{v}}_2 = \frac{e^2}{m^2 c}\left\{ - \frac{\underline{k}_2\,(\underline{E}_1\cdot\underline{E}_2)}{2w_1 k_2}\ \sin\left[[w_2-w_1]t - [\underline{k}_2-\underline{k}_1]\cdot\underline{r}\right]\right.$$

$$\left. + \frac{\underline{k}_1\,(\underline{E}_1\cdot\underline{E}_2)}{2w_2 k_1}\ \sin\left[[w_2-w_1]t - [\underline{k}_2-\underline{k}_1]\cdot\underline{r}\right]\right\}$$

We use $k_2 = \frac{w_2}{c}$ and $k_1 = \frac{w_1}{c}$, and define $w_2-w_1 \equiv \Delta w$ and $\underline{k}_2-\underline{k}_1 \equiv \underline{\Delta k}$. The acceleration can then be written:

$$\underline{A} \equiv \dot{\underline{v}}_2 = - \frac{e^2}{m^2}\,\underline{E}_1\cdot\underline{E}_2\ \frac{\Delta k}{2w_1 w_2}\ \sin(\Delta w t - \underline{\Delta k}\cdot\underline{r})$$

Now include this acceleration term, along with that due to the self-consistent field $\underline{E}_L$, in the Vlasov equation to find the resultant density fluctuation:

$$\frac{\partial f_1}{\partial t} + \underline{v}\cdot\frac{\partial f_1}{\partial \underline{r}} - \frac{e}{m}\,\underline{E}_L\cdot\frac{\partial f_M}{\partial \underline{v}} + \underline{A}\cdot\frac{\partial f_M}{\partial \underline{v}} = 0$$

where:

$$\nabla \cdot \underline{E}_L = 4\pi\rho_1(\underline{r},t)$$

and

$$\rho_1 = - en_e \int f_1(\underline{r},\underline{v},t)\, d\underline{v} \quad .$$

The solution to the Vlasov equation is simpliified greatly if we work with the Fourier components:

$$-iw\, \tilde{f}_1 + i\, \underline{k}\cdot\underline{v}\, \tilde{f} \; - \frac{e}{m}\, \tilde{\underline{E}}_L \cdot \frac{\partial f_M}{\partial \underline{v}} + \tilde{\underline{A}} \cdot \frac{\partial f_M}{\partial \underline{v}} = 0$$

where the tilde denotes transformed quantities:

$$\tilde{\underline{E}}_L(\underline{k},w) = - i\, 4\pi\tilde{\rho}_i\, \frac{\underline{k}}{k^2}$$

$$\tilde{\rho}_1(\underline{k},w) = - en_e \int \tilde{f}_1(\underline{k},\underline{v},w)\, d\underline{v}$$

$$\tilde{\underline{A}}(\underline{k},w) = - \frac{e^2}{m^2}\, \underline{E}_1 \cdot \underline{E}_2\, \frac{\Delta\underline{k}}{2w_1w_2}$$

$$\cdot \frac{(2\pi)^4}{2i} \quad \cdot \left[\delta(w+\Delta w)\;\; \delta(\underline{k}+\Delta\underline{k}) \; - \delta(w-\Delta w)\;\; \delta(\underline{k}-\Delta\underline{k}) \right]$$

By rearranging the transformed equation for $\tilde{f}_1$ and integrating over $\underline{v}$, we can get an expression for

$$\tilde{n}_1 \ (\underline{k},w) \equiv \frac{\tilde{\rho}_1}{e} \quad ,$$

the density fluctuation:

$$\tilde{f}_1 = \frac{\frac{e}{m} \tilde{\underline{E}}_L \cdot \frac{\delta f_M}{\delta \underline{v}} - \tilde{\underline{A}} \cdot \frac{\delta f_M}{\delta \underline{v}}}{-i \ (w - \underline{k} \cdot \underline{v})}$$

$$\tilde{n}_1 \ (\underline{k},w) = n_o \int \tilde{f}_1 \ (\underline{k},\underline{v},w) \ dv \quad .$$

We see that two integrals arise

(i) $$\frac{n_o e \ 4\pi \ \tilde{n}_1 \ e}{m \qquad k^2} \int \frac{\underline{k} \cdot \frac{\delta f_M}{\delta \underline{v}}}{w - \underline{k} \cdot \underline{v}} \ d\underline{v}$$

We recall that the electronic dielectric constant is given by:

$$\varepsilon_L \ (\underline{k},w) = 1 - \frac{w_p^{\ 2}}{k^2} \int \frac{\underline{k} \cdot \delta f_M / \delta \underline{v}}{w - \underline{k} \cdot \underline{v}} \ d\underline{v}$$

and hence the integral becomes:

$$\tilde{n}_1 \, (1 - \varepsilon_L) \quad .$$

(ii)
$$n_0 \frac{e^2}{m^2} \, \underline{E}_1 \cdot E_2 \, \frac{(2\pi)^4}{4 w_1 w_2} \int \frac{\underline{\Delta k} \cdot \frac{\delta f_M}{\delta \underline{v}}}{w - \underline{k} \cdot \underline{v}} \, d\underline{v}$$

$$\cdot \left[\delta(w+\Delta w) \; \delta(\underline{k} + \underline{\Delta k}) \; - \; \delta(w-\Delta w) \; \delta(\underline{k} - \underline{\Delta k}) \right]$$

We note that

$$\int \frac{\underline{\Delta k} \cdot \frac{\delta f_M}{\delta \underline{v}}}{w - \underline{k} \cdot \underline{v}} \; \delta(\underline{k} + \underline{\Delta k}) \; d\underline{v}$$

$$= \delta(\underline{k} + \underline{\Delta k}) \int \frac{- \, \underline{k} \cdot \frac{\delta f_M}{\delta \underline{v}}}{w - \underline{k} \cdot \underline{v}} \, d\underline{v}$$

$$= - \, (1 - \varepsilon_L) \frac{k^2}{w_p^{\,2}} \, \delta(\underline{k} + \underline{\Delta k}) \quad ,$$

and:

$$\int \frac{\underline{\Delta k} \cdot \frac{\delta f_M}{\delta \underline{v}}}{w - \underline{k} \cdot \underline{v}} \; \delta(\underline{k} - \underline{\Delta k}) \; d\underline{v}$$

$$= \delta(\underline{k} - \underline{\Delta k}) \int \frac{\underline{k} \cdot \frac{\delta f_M}{\delta \underline{v}}}{w - \underline{k} \cdot \underline{v}} \; d\underline{v}$$

$$= (1 - \varepsilon_L) \frac{k^2}{w_p^2} \delta(\underline{k} - \underline{\Delta k}) \quad ,$$

Hence the final equation for the density fluctuation is:

$$\tilde{n}_1(\underline{k}, w) = \tilde{n}_1 \left[1 - \varepsilon_L(\underline{k}, w) \right] + \frac{n_o e^2}{m^2} \underline{E}_1 \cdot \underline{E}_2$$

$$\cdot \frac{(2\pi)^4}{4 w_1 w_2} \left[- (1 - \varepsilon_L) \frac{k^2}{w_p^2} \delta(w + \Delta w) \; \delta(\underline{k} + \underline{\Delta k}) \right.$$

$$\left. - (1 - \varepsilon_L) \frac{k^2}{w_p^2} \delta(w - \Delta w) \; \delta(k - \underline{\Delta k}) \right]$$

or:

$$\frac{\tilde{n}_1(\underline{k},w)}{n_0} = -\frac{e^2}{m^2}\,\underline{E}_1\cdot\underline{E}_2\,\frac{k^2}{4w_1w_2w_p{}^2}\,\frac{1-\varepsilon_L}{\varepsilon_L}$$

$$\cdot\,(2\pi)^4\cdot\left[\delta(w+\Delta w)\;\delta(\underline{k}+\Delta\underline{k}) + \delta(w-\Delta w)\;\delta(\underline{k}-\Delta\underline{k})\right]$$

In terms of the space and time variables:

$$\frac{n_1(\underline{r},t)}{n_0} = -\frac{e^2}{m^2}\,\underline{E}_1\cdot\underline{E}_2\frac{\Delta k^2}{2w_1w_2\;w_p{}^2}\,\frac{1-\varepsilon_L(\Delta k,\Delta w)}{\varepsilon_L(\Delta\underline{k},\Delta w)}$$

$$\cdot\,\cos(\Delta wt - \Delta\underline{k}\cdot\underline{r})$$

Thus we see that the interaction between two electromagnetic waves in a plasma can generate a well-defined longitudinal wave in the direction $\Delta\underline{k}$. The maximum amplitude of this fluctuation is:

$$\varepsilon = \frac{e^2}{m^2}\,\underline{E}_1\cdot\underline{E}_2\,\frac{\Delta k^2}{2w_1w_2\;w_p{}^2}\,\frac{1-\varepsilon_L(\Delta\underline{k},\Delta w)}{\varepsilon_L(\Delta\underline{k},\Delta w)}$$

D. SCATTERING FROM A MACROSCOPIC WAVE

We have calculated that the interaction of two laser beams in a plasma can produce a density fluctuation:

$$n(\underline{r},t) = n_o\left[1+\varepsilon \cos(\Delta wt - \underline{\Delta k}\cdot\underline{r})\right]$$

In order to determine the magnitude of this generated wave one of the most convenient diagnostic techniques is laser scattering. To find the amount of light scattered from such a macroscopic wave, it is most convenient to calculate the density auto correlation function:

$$C_n(\underline{\Delta},\tau) = \frac{1}{Vs}\int_{Vs} d\underline{r}\,\frac{1}{T}\int_{-T/2}^{T/2} dt\;\; n_o{}^2\left[1+\varepsilon \cos(\Delta wt-\Delta\underline{k}\cdot\underline{r})\right]$$

$$\cdot\left[1+\varepsilon \cos(\Delta w[t+\tau] - \underline{\Delta k}\cdot[\underline{r}+\underline{\Delta}])\right]$$

The integrand can be rewritten:

$$n_o^2\Big[1+\varepsilon\cos(\Delta w[t+\tau] - \underline{\Delta k}\cdot[\underline{r}+\underline{\Delta}])$$

$$+\varepsilon\cos(\Delta wt - \underline{\Delta k}\cdot\underline{r})$$

$$+\varepsilon^2\cos(\Delta w[2t+\tau] - \underline{\Delta k}[2\underline{r}+\underline{\Delta}])$$

$$+\varepsilon^2\cos(\Delta w\tau - \underline{\Delta k}\cdot\underline{\Delta})\Big]$$

We see that upon averaging over a long (compared to $\frac{1}{\Delta w}$) time T and over a large (compared to $\frac{1}{\Delta k}$) volume V_s the terms depending on $\underline{r}$ and t approach zero. Only the terms independent of $\underline{r}$ and t remain, and give:

$$C_n(\underline{\Delta},\tau) = n_o^2\left[1+\varepsilon^2\cos(\Delta w\tau - \underline{\Delta k}\cdot\underline{\Delta})\right] \quad .$$

The scattered power is then given by:

$$P_s(\underline{k},w)\, dwd\Omega = r_o^2(1-\cos^2\theta)\, F_i\, V_s$$

$$\cdot\, \mathcal{F}\left\{C_n(\underline{\Delta},\tau)\right\}\, dwd\Omega$$

$$= r_o^2(1-\cos^2\underline{\theta})F_i\ V_s\ \ n_o^2\ dwd\Omega$$

$$\cdot\ \frac{(2\pi)^4}{2}\Big[\delta(w-w_o)\ \delta(\underline{k}-\underline{k}_o)$$

$$+\ \varepsilon^2\ \delta(w-w_o-\Delta w)\ \delta(\underline{k}-\underline{k}_o-\underline{\Delta k})$$

$$+\ \varepsilon^2\ \delta(w-w_o+\Delta w)\ \delta(\underline{k}-\underline{k}_o+\underline{\Delta k})\Big]$$

The first term in the bracket [ ] represents the straight-ahead scattering with no change in frequency (and is then considered "unscattered"). The last two terms represent light which is scattered out of the incident beam by the wave in the plasma. Since $\underline{k}$,w and $\underline{k}_o$,w_o are transverse electromagnetic waves they obey the dispersion relations:

$$k^2c^2 = w^2 - w_p^2 \simeq w^2$$

$$k_o^2c^2 = w_o^2 - w_p^2 \simeq w_o^2 \quad ,$$

and the scattering can be pictured as shown in fig. 2-3.

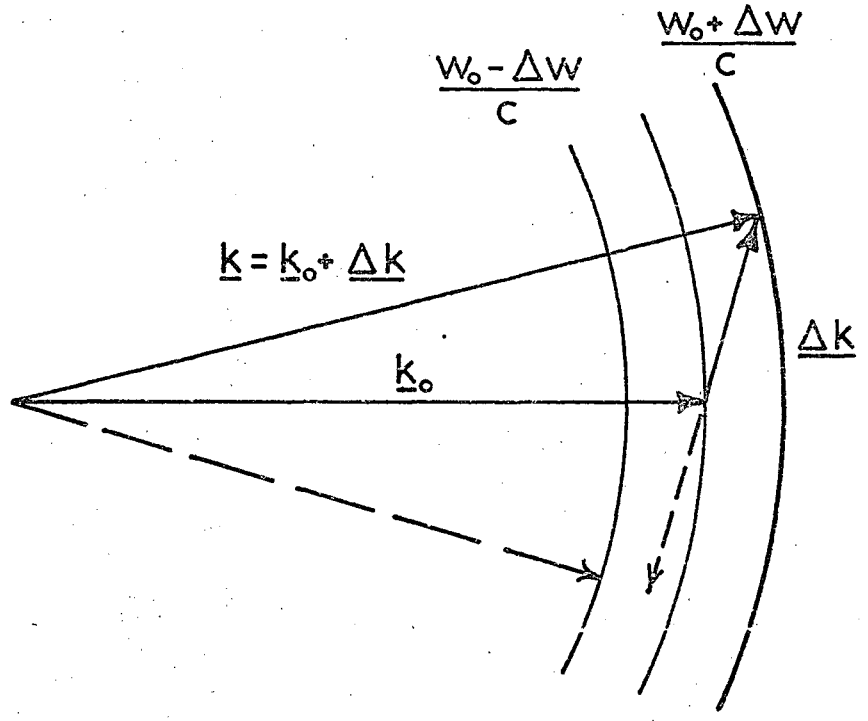

Fig. 2-3

SCATTERING FROM A MACROSCOPIC WAVE; VECTOR RELATIONS

Since $\Delta\underline{k}$ is specified by the mixing beams, the vector relations for observing only one of the satellites can be satisfied for any given $\underline{k}_o$.

This means that if beams $\underline{k}_1$ and $\underline{k}_2$ generate a wave, we cannot scatter either of these two original beams without a mismatch. In order to satisfy all the vector relations

we must have $\underline{k}_1$, $\underline{k}_2$ and $\Delta\underline{k}$ forming a closed triangle, and $\underline{k}_o$, $\underline{k}$ and $\Delta\underline{k}$ also forming a closed triangle as shown in fig. 2-4.

At the resonance $w = w_o \pm \Delta w$ and $\underline{k} = \underline{k}_o \pm \Delta\underline{k}$ the scattered intensity becomes infinitely large although the beam angle goes to zero. This result is clearly the consequence of allowing V_s to become infinitely large in performing the Fourier transform. To determine the effect of a finite scattering volume we need to consider more carefully the integral:

$$\int_{V_s} d\underline{\Delta} \; e^{-i(\underline{k}-\underline{k}_o-\Delta\underline{k})\cdot\underline{\Delta}}$$

$$\simeq \left[\int_{-\ell/2}^{\ell/2} dx \; e^{-i\,\delta k x} \right]^3$$

$$= \ell^3 \left[\frac{\sin\left(\frac{\delta k \ell}{2}\right)}{\left(\frac{\delta k \ell}{2}\right)} \right]^3$$

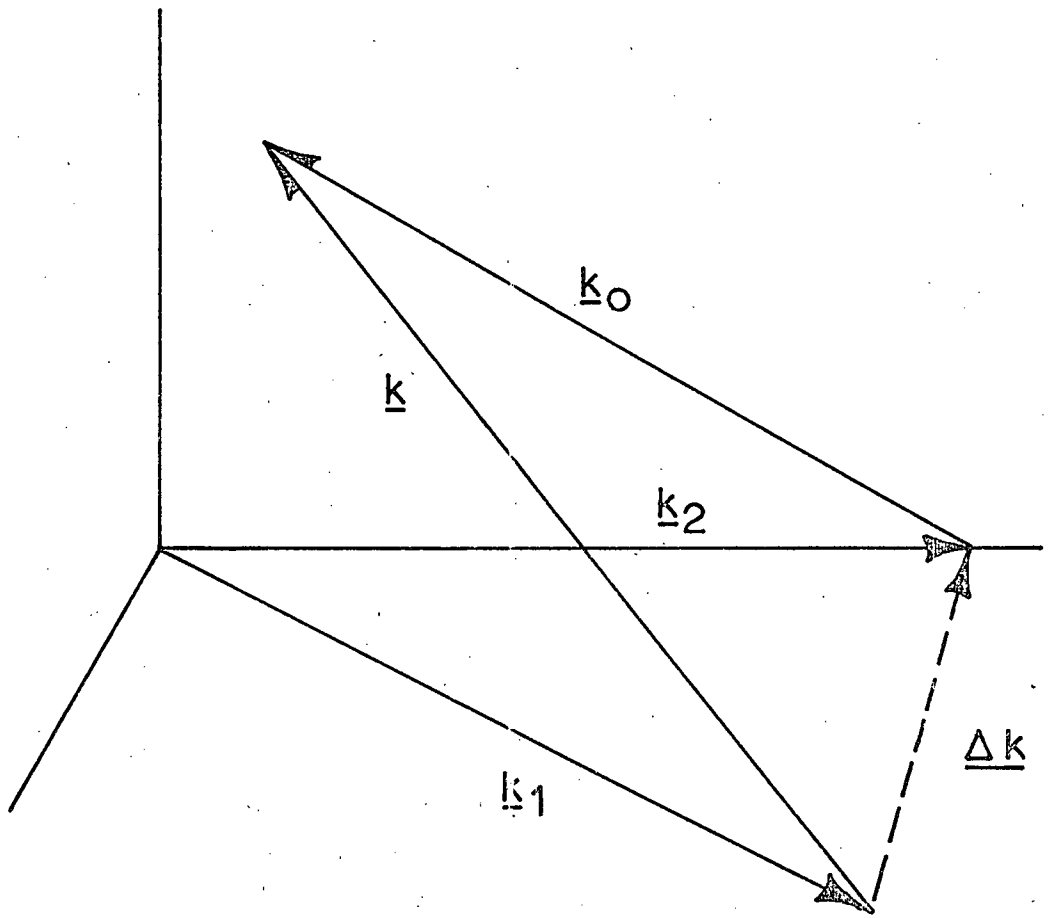

Fig. 2-4

WAVE MIXING AND ANALYSIS

$$= V_s \left[\frac{\sin \psi}{\psi} \right]^3$$

where $\Delta \underline{k}$ is the slight mismatch from the exact resonance, and $\psi = \frac{\delta k \ell}{2}$.

The scattering distribution will appear as in Fig. 2-5

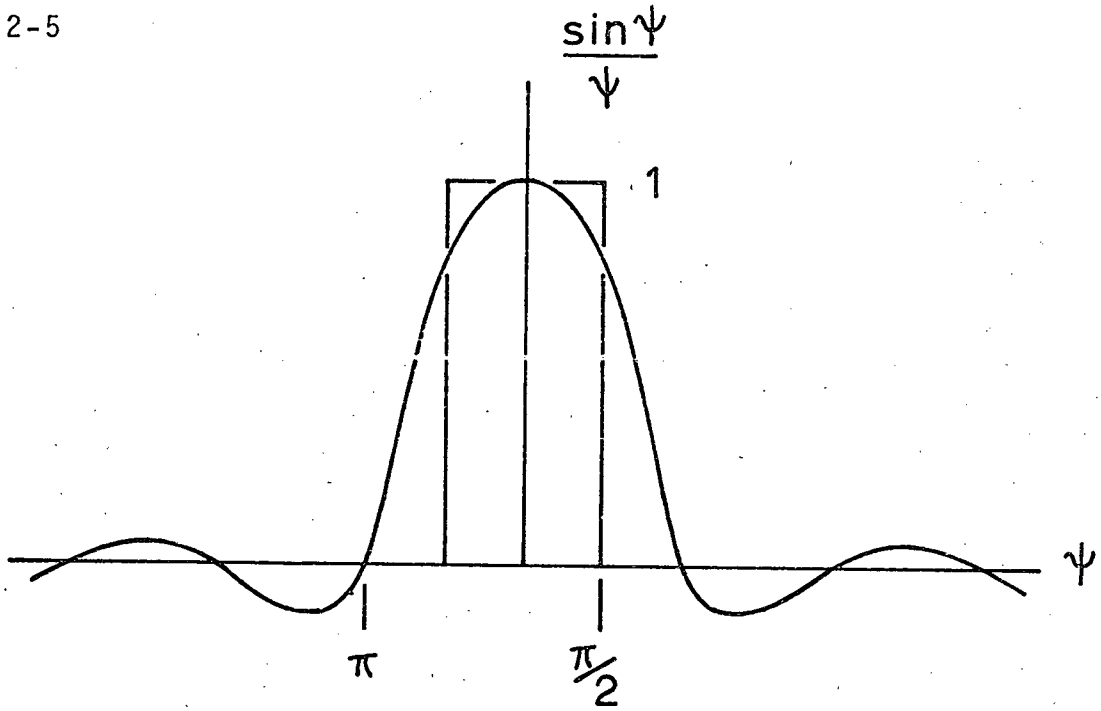

Fig. 2-5

SCATTERING DISTRIBUTION FROM A FINITE VOLUME

$$\psi = \frac{\delta k \ell}{2}$$

and the scattering will be effectively within a cone of angle

$$d\Omega \simeq \left(\frac{\delta k = \frac{2\pi}{\ell}}{k_o} \right)^2 .$$

i.e. $$d\Omega \simeq \frac{4\pi^2}{\ell^2 k_o^2}$$

This angle is essentially the cone angle due to diffraction from the volume $V_s = \ell^3$.

The scattered power is given by:

$$\int_{\text{aperture}} \int_{\text{freq.}} P_s(\underline{k},w)\, dw d\Omega$$

$$= r_0^2(1-\cos^2\theta)\, S_i\, V_s\, n_o^2 \varepsilon^2 2\pi \int \delta(w-w_o-\Delta w)$$

$$* V_s \frac{4\pi^2}{L^2 k_o^2}\, dw$$

$$= r_0^2(1-\cos^2\theta)\, S_i\, (n_o V_s)^2\, \varepsilon^2\, 2\pi \frac{4\pi^2}{L^2 k_o^2}$$

where the aperture includes all of the diffracted cone.

We see that the scattered power is strongly dependent upon the fluctuation ε, so it is of considerable

importance that we determine the scattered power, compared to the scattering due to thermal fluctuations. It has been pointed out by Weinstock (1967) that the coherent scattering (which we considered here) and the incoherent scattering due to the thermal fluctuations are independent, and hence are simply additive.

For the He plasma used for this experiment, the density is $\simeq 2.2\times10^{16}$ cm^{-3}, and the temperature is $\simeq$ 17,000 K. The scattering (and mixing) angle is 45°. These parameters give for the fluctuation amplitude:

$$\varepsilon = \frac{e^2}{m^2} \underline{E}_1 \cdot \underline{E}_2 \frac{1-\varepsilon_L}{\varepsilon_L} \frac{\Delta k^2}{\Delta w^2} \frac{1}{w_1 w_2}$$

where:

$$\Delta k \simeq .65\times10^{5} \text{ cm}^{-1}$$

$$\Delta w \simeq 9.6\times10^{12} \text{ sec}^{-1}$$

$$w_1 \simeq w_2 \simeq 2.55\times10^{15} \text{ sec}^{-1}$$

$$\frac{1-\varepsilon_L}{\varepsilon_L} \simeq 5 \text{ at the maximum.}$$

For an electric field of 10^3 $esu/_{cm}$, this produces $\varepsilon \simeq 2.0\times10^{-5}$, and a scattered power

$$\frac{P_s}{P_i} = \varepsilon^2 r_0^2 (1-\cos^2\theta)\ (n_o V_s)^2$$

$$\cdot\ \frac{2\pi^3}{L^2 k_o^{\ 2}}\ \ \frac{1}{L^2}$$

$$\simeq 5 \times 10^{-14}$$

This scattered power is comparable to that scattered from the thermal fluctuations (see section B, page 10), and hence should be observable.

E. CRITICAL ANALYSIS OF EXPERIMENTAL PROPOSALS

It is obvious that for the wave-mixing process to be of any interest it must be observable, and hence one must examine the size of the signal received by some detector.

In their original paper, Kroll, Ron and Rostoker (1964) have assumed an extremely large value for the electric fields (10^8 V/cm, which is produced by a 10 Gigawatt laser focused to a 200μ diameter spot) in order to achieve an enhanced cross-section

$$\frac{\sigma_{enh}}{\sigma_{th}} \simeq 10^{13}\ ,$$

where σ_{th} is the (thermal) differential cross-section for scattering in the electron satellite. They then calculate the flux density of the scattered beam and find

$$\frac{F_s}{F_i} \simeq .3\times10^{-6} \quad ,$$

where F_s and F_i are the scattered and incident flux densities. A calculation of the flux density is really not meaningful, however, since a very small cone angle gives large flux densities but very small signals. One detects fluxes, and to compare the enhanced scattering with the thermal scattering, for example, we must know the cone angle $d\Omega$. The scattered power is then $P_s = A\,F_s = r^2 d\Omega F_s$; where the collecting aperture has an area larger than A at a distance r. For the mixing process, the cone angle is the diffraction angle, and for a 1 mm diameter gives $d\Omega \simeq 5\times10^{-7}$ Sr. Hence the scattering ratio

$$\left(\frac{P_s}{P_i}\right)_{enh} = \frac{F_s}{AF_i} = 1.5\times10^{-7} \quad .$$

Since $\left(\frac{P_s}{P_i}\right)_{thermal} \simeq 1.6\times10^{-14}$, one should readily detect the enhanced signal. For a more reasonable, but still large, value for the electric field (say $\simeq 10^6$ V/cm) we find:

$$\left(\frac{P_s}{P_i}\right)_{enh} \simeq 1.5\times10^{-15} \quad ,$$

or only 10% of the thermal satellite intensity. Such considerations indicate that the plasma chosen by Kroll, Ron and Rostoker would be an unlikely candidate for any wave-mixing experiment.

There are, in addition, two factors which can adversely affect the size of the fluctuation produced: electron density gradients and broad laser lines.

If the density is not constant throughout the focal volume, the resonance is smeared out. In order for such detuning to be small, we should have $\Delta w_p < \Delta w_{res}$, where Δw_p is the change of w_p through the focal volume due to density gradient, and Δw_{res} is the width of the resonance for a constant density. In the situation chosen by Kroll, Ron and Rostoker, the resonance is very sharp:

$$\Delta w_{res}/w_p \simeq 10^{-3} \quad ,$$

and hence within the focal volume it would require

$$\Delta w_p/w_p \simeq 10^{-3} \quad ,$$

or

$$\Delta n/n \lesssim 2\times10^{-3} \quad .$$

It is very unlikely that one would encounter a plasma constant in density to 0.2% over a length of 1mm.

If the laser linewidth Δw_L is not small compared to the width of the resonance Δw_{res}, only a fraction

$$\left(\simeq \Delta w_{res} / \Delta w_L \right)$$

of the laser power will be useful in driving fluctuations. In Kroll, Ron and Rostoker's work, they assumed $n_e \simeq 10^{14}$ cm^{-3} and hence w_p corresponds to a shift of 2Å. In order to use all the laser power, we need $\Delta\lambda_L \simeq 2.10^{-3}$ Å. Such a narrow linewidth is never achieved with high-power lasers, a width of .01Å being very good.

In a proposal by Bradley, Magyar and Richardson (1965), they describe an experiment designed for wave-mixing, using two high-powered ruby lasers, incident at a shallow angle ($\sim 4.6°$), with a plasma of density $n_e \simeq 9\times10^{14}$ cm^{-3}. The expected satellite shift was about 5Å, and the resonance was less sharp than that assumed by Kroll, Ron and Rostoker:

$$\Delta w_{res} / w_p \simeq 10^{-2}.$$

In this case $\Delta\lambda_L$ was required to be less than 0.05Å (a difficult but not impossible problem), and the density was hopefully constant to about 1% through the focal volume of $1mm^3$.

Even the large fields assumed (10^7V/cm, equivalent to a 100MW beam focused to a 200μ dia. spot) would only produce a scattered ratio

$$\frac{P_s}{P_i} \simeq 10^{-12} .$$

A more likely laser power is 10MW, focused to a 300μ spot. This results in a field of 2×10^6 V/cm ($\sim10^4$esu/cm). Such a laser used in the plasma anticipated by Bradley, Magyar and Richardson would give

$$\frac{P_s}{P_i} \simeq 10^{-16} ,$$

with little hope for detection.

With a plasma of higher density (say 2×10^{16} cm^{-3}) one can eliminate many of these experimental difficulties. It is shown in the previous section on laser scattering from a macroscopic wave that a rather feeble laser producing a field of 10^3 esu/cm (a 1 MW beam focused to 300μ) could produce a scattered power

$$\left(\frac{P_s}{P_i}\right)_{enh} \simeq 5\times10^{-14} ,$$

which is comparable to the scattering from thermal fluctuations. In addition, for the plasma chosen ($n_e \simeq 2.2 \times 10^{16}$ cm^{-3} and T $\simeq$ 17,000 K) the resonance is much broader so the conditions on the density gradients and laser linewidth are not at all severe.

CHAPTER III

THE EXPERIMENT

We may consider the experiment to observe nonlinear wave-mixing to consist of two parts; firstly the plasma wave must be produced, and secondly it must be detected. The two laser beams used to generate the plasma wave are produced in a dual-cavity organic dye laser. These two beams are focused into the same spot in the plasma, and the longitudinal wave is generated in the intersection of the focal volumes. In order to detect the generated wave we scatter a third beam from this same small interaction volume and observe the spectrum of the scattered light. The third beam we use is the remnant ruby laser beam which passes through the dye cell. The spectrum near the ruby wavelength is examined with a monochromator and photomultiplier detection system. The presence of the plasma wave will manifest itself as a change in intensity of one of the electron thermal satellites.

An illustration showing the basic features of the experiment is given in fig. 3-1.

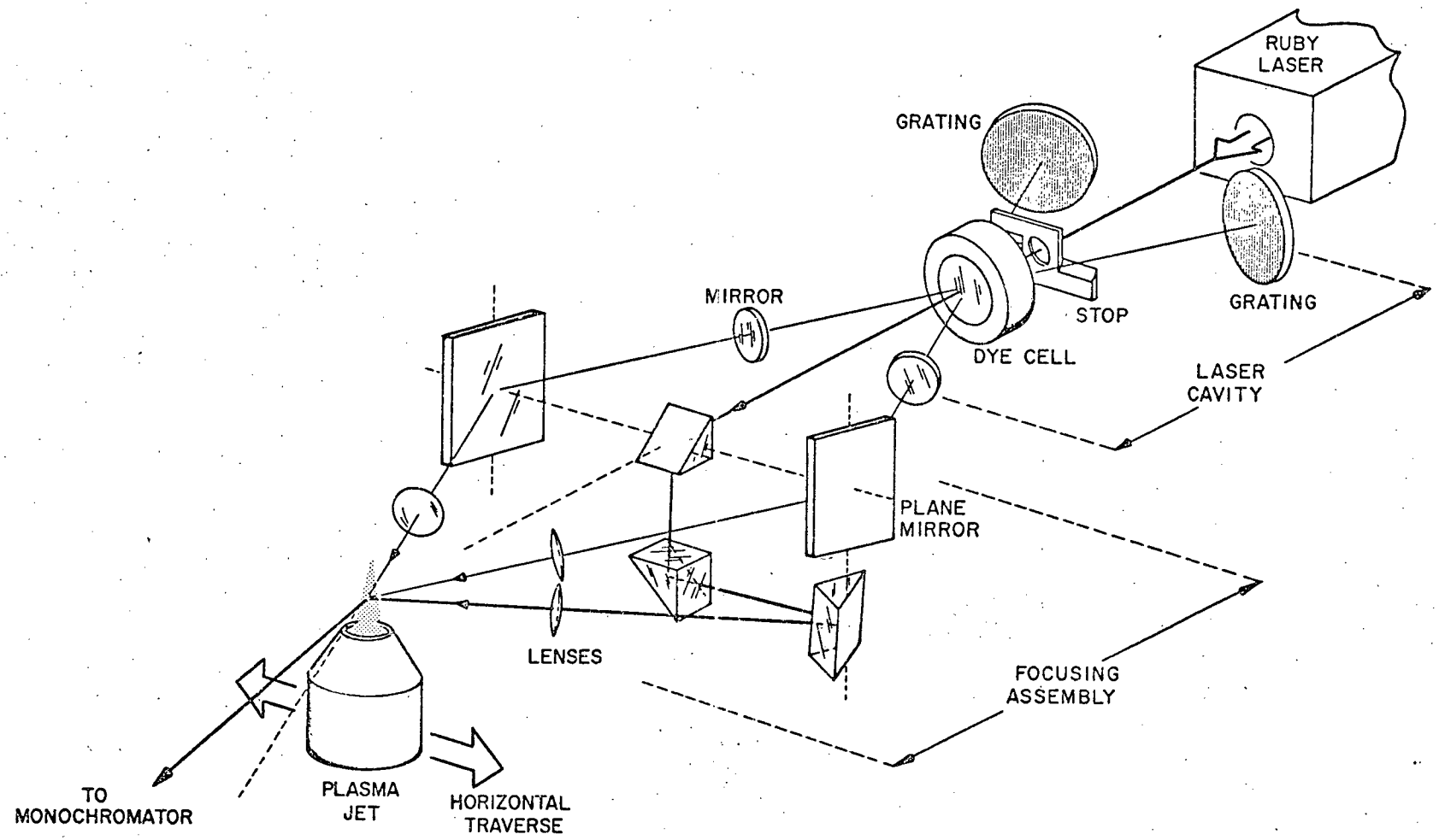

Fig. 3-1

ILLUSTRATION OF THE EXPERIMENT

THE APPARATUS

A. THE RUBY LASER

The ruby laser used in this experiment was the one developed in this laboratory by M.T. Churchland (1969) and is described well in his thesis. The ruby rod is 6" long, 1/2" in diameter with Brewster-angle ends. It is pumped in a double-elliptic housing by two linear flashlamps, with a total bank energy of about 3500 J. Both the ruby and the flashlamps are water cooled. The optical resonant cavity is formed by 99.9% and 30%-reflecting dielectric-coated mirrors. The Q-switching element is a bleachable dye, in this case a solution of cryptocyanine in methanol, in a Brewster-angle cell.

The laser is capable of producing pulses containing 1.5 joules, with a pulse duration of 20 to 30 nanosec.

B. THE DYE LASER

Since cryptocyanine was readily available, it was decided to use cryptocyanine, dissolved in glycerin to form a 3×10^{-5} molar solution, as the lasing medium. A solution of cryptocyanine in iso-amyl alcohol was also tried, but was found to produce only about one-half of the power of the glycerin-based laser. It became obvious during the course of the work that cryptocyanine was not the best possible choice for several reasons. The dye is quite delicate and breaks down under the action of the ruby

laser light and thermal agitation (to a marked degree in the less viscous iso-amyl alcohol).

The dye cell (shown in fig. 3-2) was machined from aluminum, with 2-inch diameter optical flats (supplied A. Jaegers) containing a 1 cm path in the liquid. This short cell was chosen for two reasons:

(i) The ruby beam heats the solution, and a train of bubbles is formed in the glycerin. Glycerin being very viscous, these small scattering centers remain in the optical path and both degrade the performance of the dye laser and scatter the ruby beam as it passes through the cell. The number of bubbles per cm of liquid doesn't seem to depend on the length of the path or on the dye concentration, so the shorter the path in the liquid the smaller the disturbance produced by the bubbles.

(ii) The dye laser is pumped in the longitudinal mode described by Bradley et. al (1968), with a 10 degree angle between the ruby beam and the axes of the dye lasers. In this configuration, the shorter the cell the greater will be the pumping efficiency.

The faces of the cell windows were purposely made non-parallel to prevent lasing from the cavity formed by plane-parallel windows.

During the course of experiments with the dye laser various cavity configurations were used. As a front

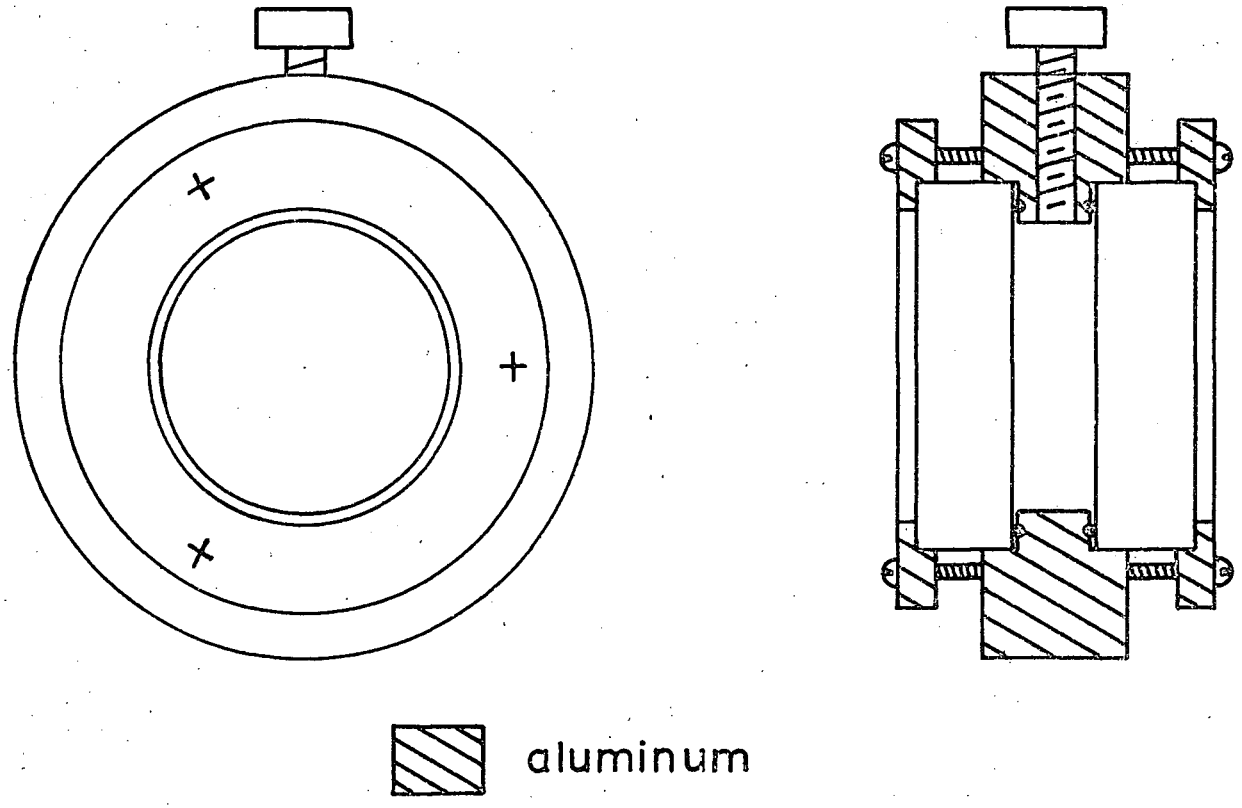

Fig. 3-2

DYE CELL CONSTRUCTION

(partially-reflecting) mirror we used sapphire etalons, aluminized quartz flats with a small (approximately 3 mm diameter) uncoated central spot, and broad-band dielectric-coated mirrors. All of these worked, but the dielectric mirrors produced by far the best output. As rear (fully-reflecting) mirrors the following have been used: plane aluminized mirrors, a 60° flint prism with an aluminized mirror, and aluminized reflection gratings. Again, all of these worked, but for our purposes the grating was an obvious necessity.

Any consideration as to which grating should be used must take into account the efficiency of the grating blaze, the laser linewidth required and the angular sensitivity. Since most of the grating losses (other than obsorption) are through zero order reflections, it is possible to use this as the laser output. The mechanical arrangement is rather more complicated, however, and it was thought best to use the first order retroreflection with a partially-transmitting mirror. In order to keep the dye laser cavity losses as low as possible, one wants a high blaze efficiency. In order to achieve as narrow a line as possible, one would like to have as many grooves per mm. as possible on the grating. In a sense, these are contradictory, since fewer grooves allows a better blaze in general, but it is advantageous to have a reasonably large number of grooves for reasons indicated below:

The dye laser linewidth must be greater than that determined by the resolving power of the grating:

$$R.\ P. \equiv \frac{\lambda}{\Delta\lambda} = nN$$

where

λ is the (peak) wavelength

$\Delta\lambda$ is the smallest resolvable wavelength difference

n is the order of interference

and N is the total number of grooves used by the beam.

Hence the linewidth $\delta\lambda \gtrsim \frac{\lambda}{R.\ P.}$. For a 1 cm. diameter dye laser beam and a grating with 1200 grooves per mm., the R.P. is 12,000, and hence near λ = 7400 Å, the linewidth must be greater than about 0.6Å. In actuality, the linewidth may be 2-3 times this. Since the plasma resonance is only about 3Å wide, we chose to use plane reflection gratings with 1200 lines /mm. to keep the laser linewidth comparable to the resonance width. The gratings are blazed for 7500 Å, with an efficiency of about 75%, and were purchased from Bausch and Lomb (catalogue number 35-53-05-360).

The ability to determine the wavelength of the laser is determined by the angular dispersion of the grating. For the grating used in this experiment the angular dispersion is:

$$\frac{d\theta}{d\lambda} = \frac{1}{2d\ \cos\theta} \simeq \frac{1\text{m rad}}{15\ \text{Å}} \quad ,$$

where d is the grating spacing

and θ is the angle of the beam from the normal to the grating surface.

This means that in order to establish the wavelength to 1.5Å we need to set the angle to within $\Delta\theta \simeq 0.1$mrad. Since this is a very small angle, we see we are led to another compromise, this time between angular sensitivity and mechanical convenience. A 0.01 mm micrometer head, which rotates the grating via a 10 cm lever arm, as shown in fig. 3-3, was used to provide the 10^{-4} radian sensitivity while maintaining reasonable solidity.

As can be seen in the diagram, it is also necessary to allow for adjustment of the grating around a normal to its surface. This allows one to align the grooves of the grating parallel to the rotation axis, which is essential to maintain alignment as we scan the grating.

C. THE OPTICS

The optical set-up is bound to be complicated, since we must focus three laser beams into a single spot in the plasma jet and we must collect scattered light for analysis.

In order to direct the dye laser beams into the plasma we must deflect and focus them. For deflection it would

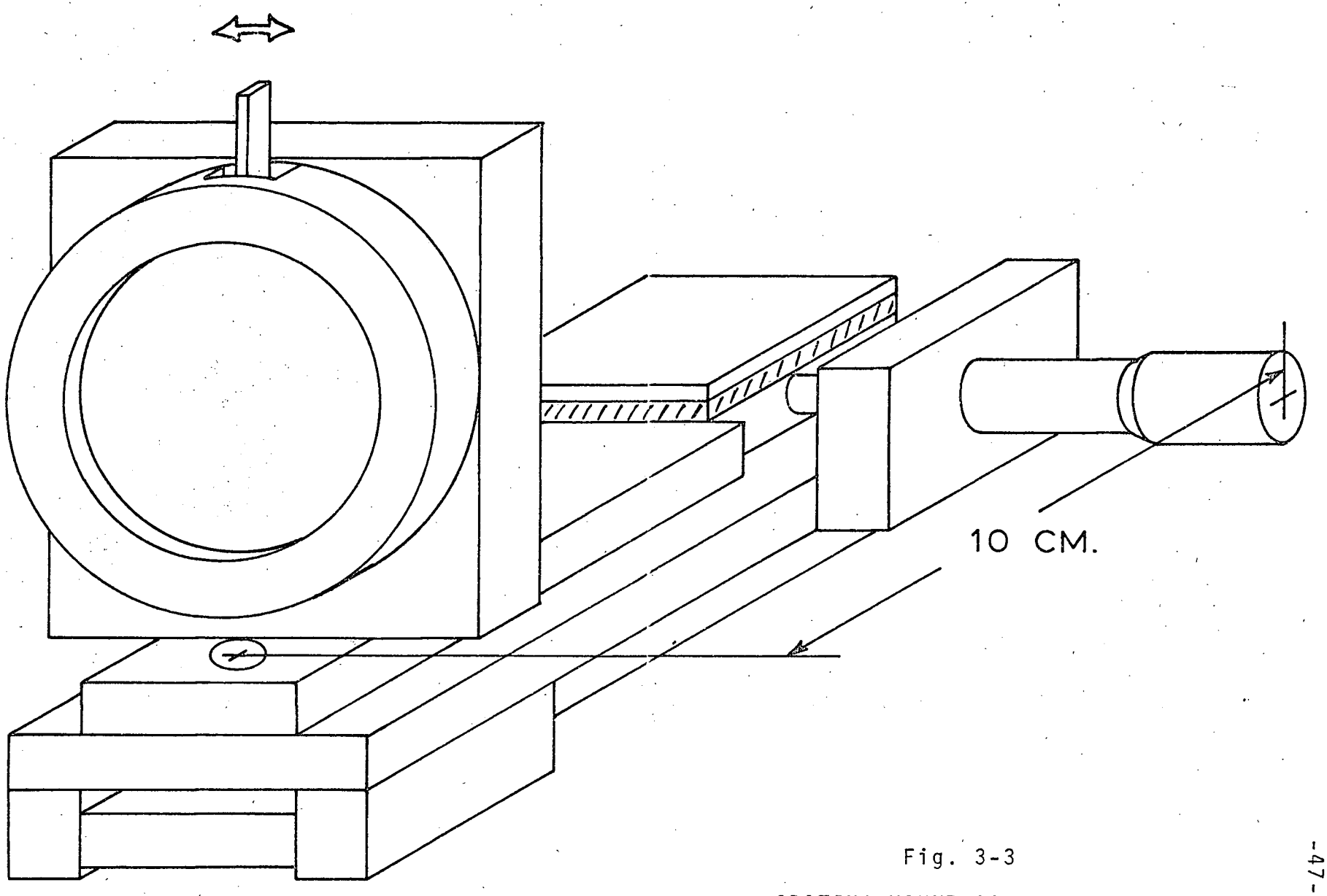

Fig. 3-3

GRATING MOUNT CONSTRUCTION

be possible to use prisms, changing the angle of deviation by rotating the prisms slightly. For the geometry used in our experiment the beams have to be deflected by about 32.5°, which requires a prism apex angle of about 25°. Prisms of such geometry are not readily available, and hence it was decided to use front-surface aluminized mirrors. Since the amount of deflection was small, the dye laser beam is incident at a large angle to the normal of the mirror (approximately 75°). The mirrors are then required to be rather large, and were made 3 inches wide in order to collect all the beam. There was little deterioration of the mirrors, but for high-powered lasers one would need to use prisms. The dye laser beams are focused by lenses with the shortest focal length compatible with the experimental geometry (about 12 cm.).

The ruby laser beam is focused into the same spot as the two dye laser beams. After passing through the dye cell, it is deflected downward by an internally-reflecting prism, across to another prism underneath the mirror deflecting the dye beam as shown in fig. 3-1, and then upward at an angle of about 13° to the horizontal into the plasma. It is focused by another reasonably-short (about 12 cm.) focal length lens.

In order to collect the scattered light, which will lie in the plane formed by ($\underline{k}_2 - \underline{k}_1$) and $\underline{k}_L$ (where $\underline{k}_1$ and $\underline{k}_2$ are the wavevectors of the dye beams, and $\underline{k}_L$ is the

wavevector of the ruby beam), a mirror is used in this plane. The mirror is slightly tilted to send the light through the collecting lens, parallel to the table-top and through the focusing lens into the monochromator. The lenses used are f/5 achromats, with focal length 15 inches and diameter 3".

The monochromator used in this experiment is a SPEX model 1800-11, which is a $\frac{3}{4}$ meter, f/6·3 instrument with the capability of being used as a spectrograph or a monochromator. It has a 1200 groove /mm. grating blazed at 7500 Å. The height of the entrance aperture was reduced to 300μ by using a sliced brass sheet in front of the slit, but the slit width remained variable. No stops are used on the exit slit, whose width was also variable.

The photomultiplier used is an RCA 7265, which has an S-20 photocathode, a large gain (about 10^7 at the voltage used in this experiment), and a good risetime (the tube used had a 6 nanosec. risetime). Near the ruby laser wavelength (6943Å) the S-20 photocathode has a quantum efficiency of about 3%. The tube is operated at a voltage such that with no filters in the path from the jet to the monochromator, the light from the jet at high current produces only a 0.2 ma anode current. This is well below the maximum long-term current rating of 1.0 ma, and also well below saturation (the chain current was 2.0 ma). In pulse mode

the photomultiplier can deliver large currents without saturation (signals of 1 volt across 25Ω were possible).

All of the laser beams are monitored by Hewlett-Packard PIN photodiodes, which receive light reflected from glass plates placed in the beams.

D. THE PLASMA JET

The plasma jet used in this experiment is similar to that used by Chan (1968) and Van der Kamp (1968), and is shown in fig. 3-4. The anode has been modified to the design developed by R.N. Morris and has a conical appearance. This suits the experiment very well since we don't want the ruby beam, coming from below, to hit any part of the jet.

Helium is used as the working gas in the jet since it is superior to Argon in two aspects vital to scattering experiments. Whereas the Argon plasma can be strongly perturbed by the laser pulse (see Van der Kamp (1968)) the Helium plasma is not noticeably affected. Another consequence of the lower density of the Helium jet is that there is considerably less continuum radiation than from an Argon plasma.

A Miller model SRH-33 welding supply is used to maintain the jet at low current (approximately 50 amps.) throughout a run. When a shot is to be taken, the current

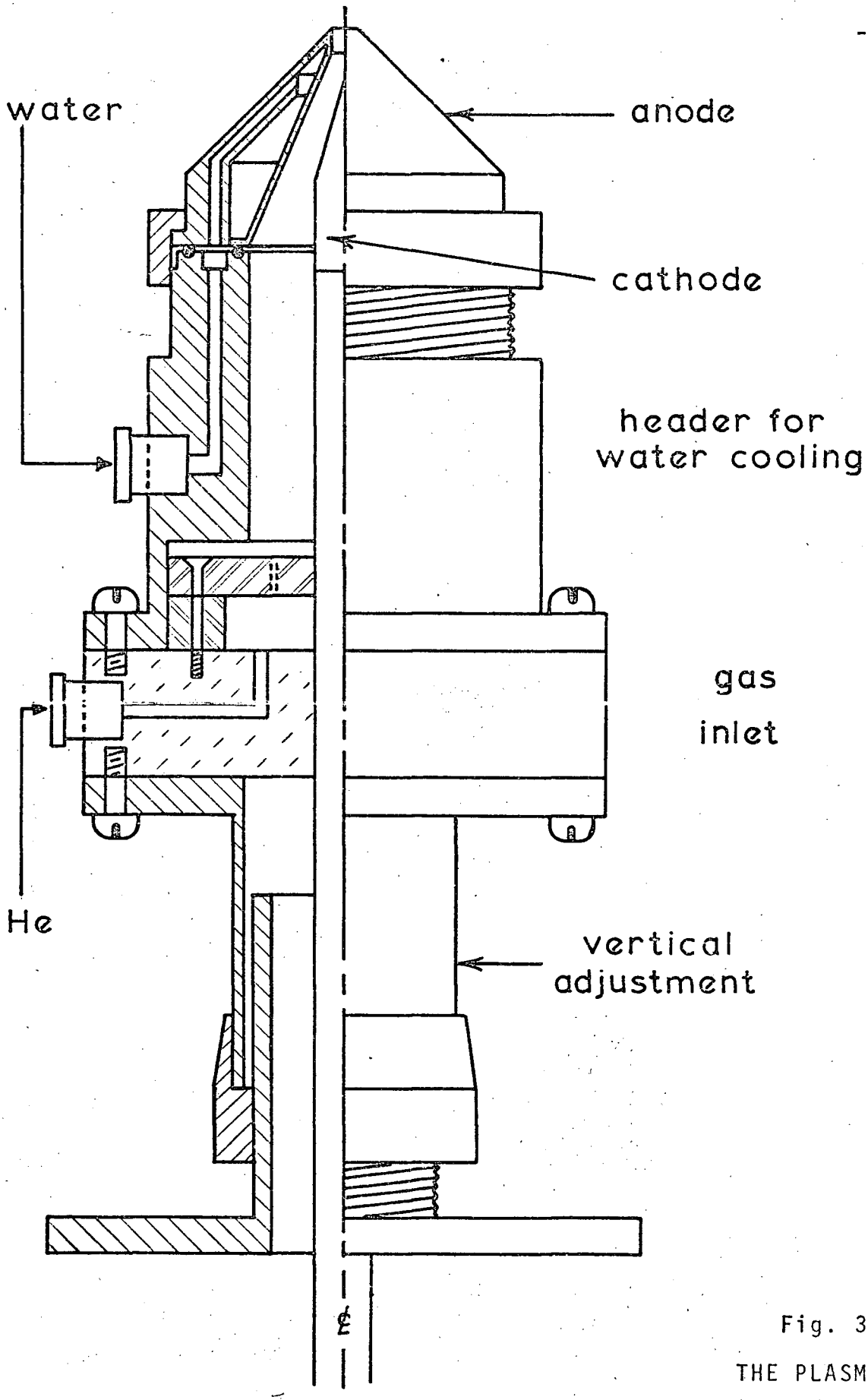

Fig. 3-4

THE PLASMA JET

is increased in stages to 250 amps., with a parallel set of 24 1-ohm ballast resistors to regulate the current. The voltage drop across the jet at high current is about 22 volts, so a bank consisting of 2 parallel sets of 4 heavy-duty lead-acid batteries is used as a high current, ripple-free source of 48 volts. The Helium plasma jet was found to run unstably when driven by a bank of 9 batteries supplying only 36 volts.

CHAPTER IV

EXPERIMENTAL RESULTS

A. DYE LASER

There are certain aspects of the dye laser which are important characteristics as far as the wave-mixing experiment is concerned: the power output, the time behaviour of the pulse, the tunability of the output and the linewidth of the laser beam. These were examined, as well as several other interesting properties of the dye laser which are worth reporting. I should note, however, that the work was done quickly since the aim of the experiment was to use the dye laser as a tool.

When the dye was pumped by a pulse from the giant-pulse ruby laser it would emit a burst of light whose time behaviour followed closely that of the pumping pulse. As well, the dye laser - like all lasing systems - is found to have a threshold. This threshold varies with the type of dye and with the quality of the resonant cavity. The dye used in this experiment (a 3×10^{-5} molar solution of cryptocyanine in glycerin) would lase, in the configuration used in the experiment, when pumped by a ruby pulse of about 0.5 joules when using an aluminized mirror and

about 0.75 joules when using the grating reflector. When the dielectric front mirror of the dye laser cavity was replaced by a sapphire etalon (peak reflectivity ~26%) the threshold increased slightly, and the spectrum of the laser output showed definite channeling due to the reflectance peaks of the etalon.

The power output of the dye laser depended on several factors, but mainly the quality of the resonant cavity (i.e. whether the gratings were in good shape or not). With one good grating, blazed at 7500Å with an efficiency ≈80%, an output of 280 mj was obtained with a pump of 1.2j (an efficiency of 23%). During the run of the experiment the gratings were deteriorating slightly due to evaporation of the aluminum coating by the laser pulse, but an input of 1.2j would consistently produce an output of 50 mj in each beam. Thus, the efficiency was not nearly as great, being about 8%. The energy output of the dye laser and the ruby laser was measured by a TRG model 101 ballistic thermopile. The power was estimated by measuring the laser pulse width (approximately 20-30 nsec., but it varies with the concentration of the dye in the Q-switching cell). The power output of the dye laser is thus about 2MW with a pump delivering 50MW.

The use of an aluminized fully-reflecting mirror results in a spectrum about 30-40Å wide, but when the

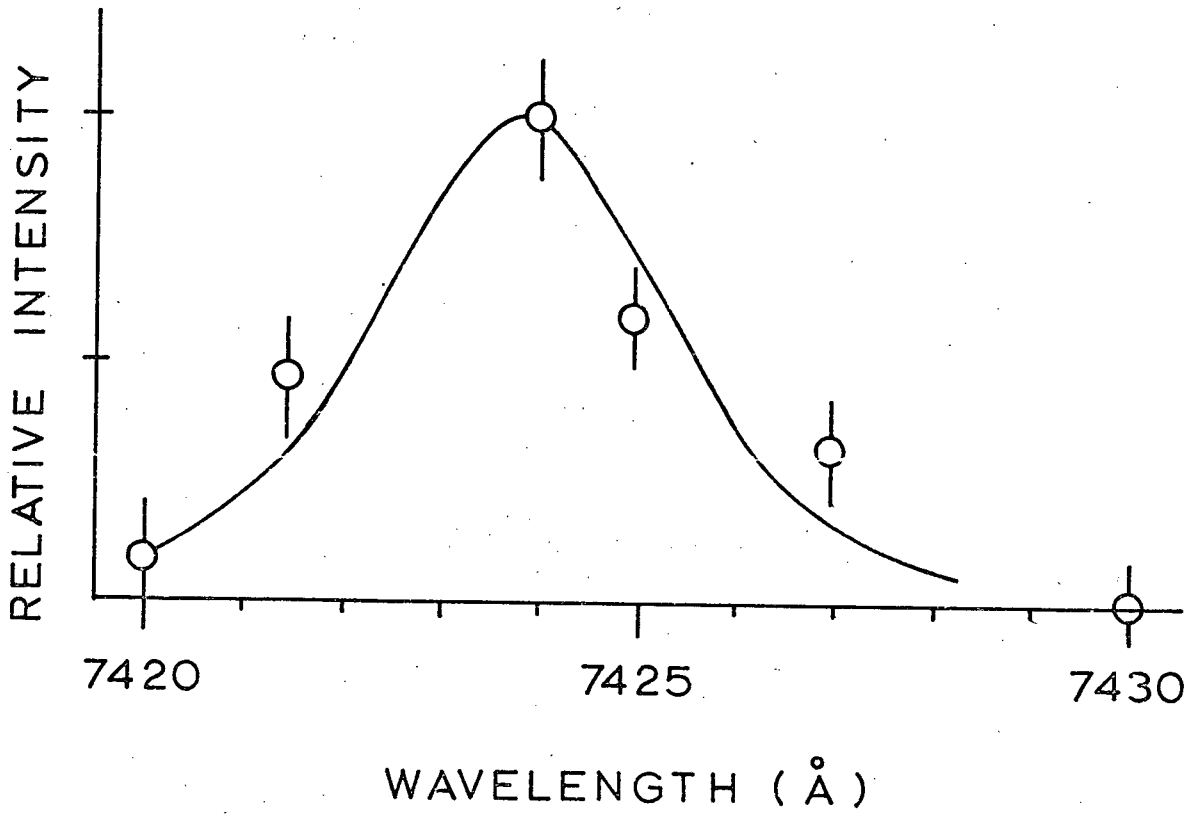

Fig. 4-1

MEASUREMENT OF DYE LASER LINEWIDTH

The smooth curve represents a convolution of the instrument profile with a 1.5Å half-width Lorentzian profile.

grating reflector is used the linewidth is reduced considerably. The linewidth was measured by scanning the monochromator through the laser line. The result is shown in fig. 4-1 (the error bars are only estimates). The theoretical curve represents the convolution of the instrument profile with a Lorentzian curve of half-width 1.5Å. It would appear that the line is skewed to the long-wavelength side, but a more careful measurement is needed.

By rotating the grating this line can be scanned over an interval of about 80Å - a larger range than appears in the broad-band spectrum. The precision with which one can establish the lasing wavelength depends on the mechanical design, and for the system used in this experiment the line should be determined to about ½Å. For fine work, more precise wavelength determination is required, and the grating would definitely not be suitable.

It was found that there was a length threshold for the dye laser. When the length of the resonator exceeded some limit, the lasing would cease altogether. The diminishing output with length (using a sapphire etalon as output mirror) is shown in fig. 4-2. For a cavity shorter than 30 cm, the output was found to be almost constant. It may be possible to explain this behaviour in two ways:

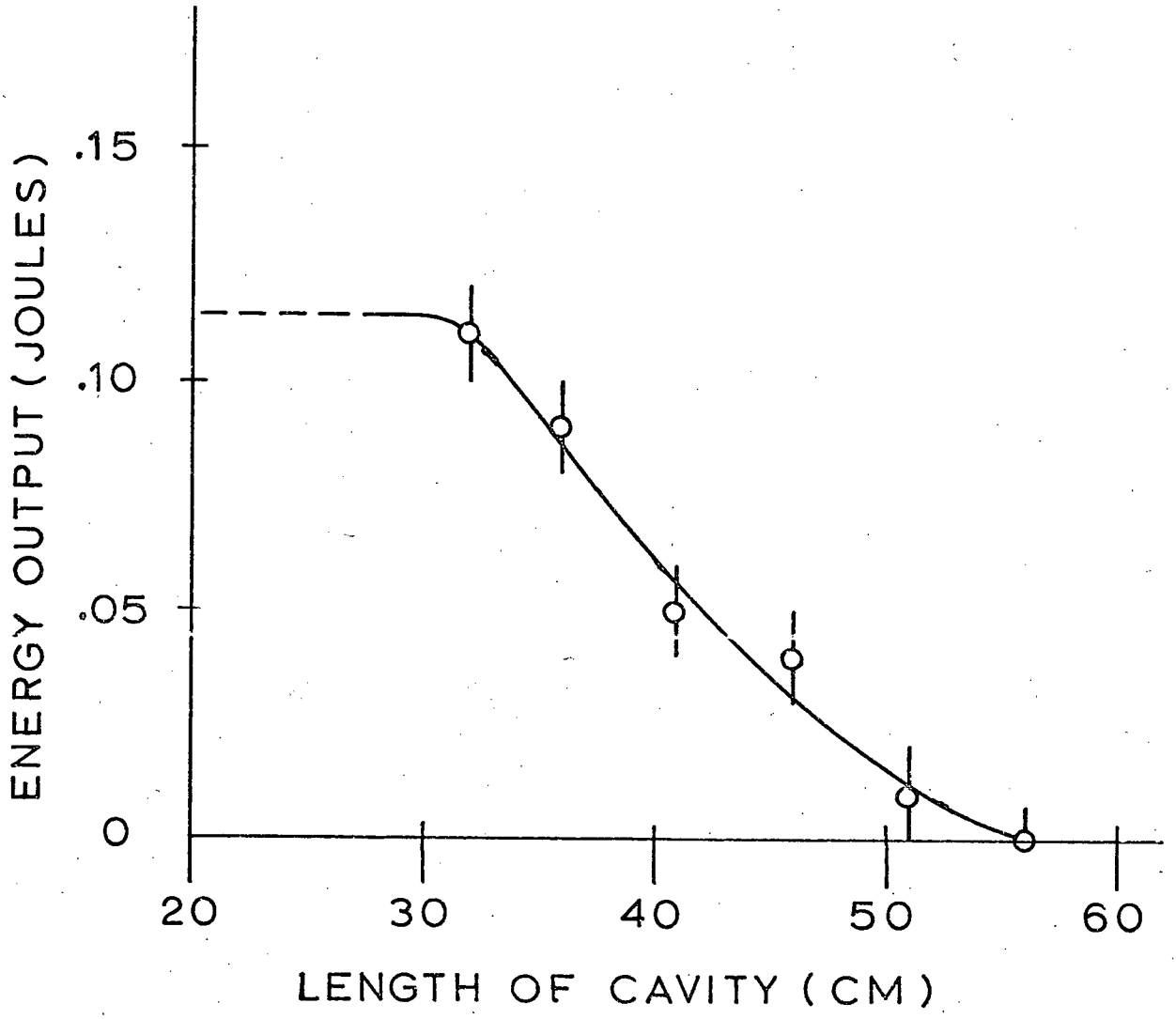

Fig. 4-2

LENGTH DEPENDENCE OF THE DYE LASER OUTPUT

(a) When the feedback provided by the resonant cavity is reduced, it will take more "transit times" of the cavity in order to build up any lasing. If this total build-up time becomes comparable to the time of the pumping pulse, then there will be little lasing action.

(b) We know that in general the fluorescent dyes have short lifetimes of the order of a few nanoseconds. If the transit time of the cavity becomes comparable to the radiative lifetime of the upper level of the dye molecule, there will be large losses due to spontaneous emission and hence lasing will cease.

It has also been found that the transmission of the ruby laser beam through the dye cell depends very strongly on the action of the dye laser. If the front mirror of the dye laser cavity is covered, the ruby light is almost completely transmitted through the cell. If the dye laser is operating a much smaller fraction is transmitted (approximately 20% for the dye concentration, cell length and cavity used for this experiment). This phenomenon is almost certainly due to the bleaching of the dye by the strong laser pulse. When there is depopulation of the upper level by lasing, the bleaching process is short-circuited and the molecule can again absorb the ruby light.

B. SCATTERING RESULTS

Basically, there are two scattering experiments involved: normal scattering without the dye lasers, and enhanced scattering with the dye lasers also focused into the plasma. The purpose of the normal scattering experiment was to establish the presence and the position of the satellite so that we can later tune the dye lasers to this resonance.

For all the runs the jet was operated under the following conditions:

Gas used	Helium
gas flow	11.8 ℓ/min
nozzle diameter	4 mm
pressure	atmospheric
Jet current	250 amps
observation angle	45°
solid angle	f/6.3 or 0.02 Sr
Band pass	300μ slits, 3Å
photomultiplier voltage	2400 V

It should be noted that no filters or polarizers were used between the jet and the monochromator. The voltage on the photomultiplier was reduced to a level where there was no saturation or danger of damaging the anode by too large a long-term current.

(i) NORMAL SCATTERING

Satellites were found symmetrically displaced on both sides of the central wavelength, but the feature on the lower-wavelength side was examined more carefully. The results are shown in fig. 4-3. The experimental points represent the means of about 4 shots at each wavelength setting. The error bars are the standard deviations of the means. The theoretical curve drawn is the convolution of the measured instrumental response with the theoretical scattering profile for a plasma with $n_e = 2.20 \times 10^{16}$ cm^{-3} and $T_e = 17000$ K. The fit of the theoretical curve to the experimental points is reasonably good, except for those points with a large shift relative to the peak. An attempt was made to produce a better fit, but the slope of the theoretical curve was consistently too steep in this region. The density gradients in the Helium jet are very small, and from the results of Van der Kamp (1968) we can estimate that $\frac{\Delta n}{n} \lesssim 2\%$ over a 300μ distance in the plasma. Thus inhomogeneities represent a very small fraction of the observed width, and an estimation of the effect of density gradients on the shape of the satellite indicates that the slope of the theoretical curve can only be steepened further. It may be necessary to include collisional damping in order to obtain a good fit for those points with shifts beyond the peak.

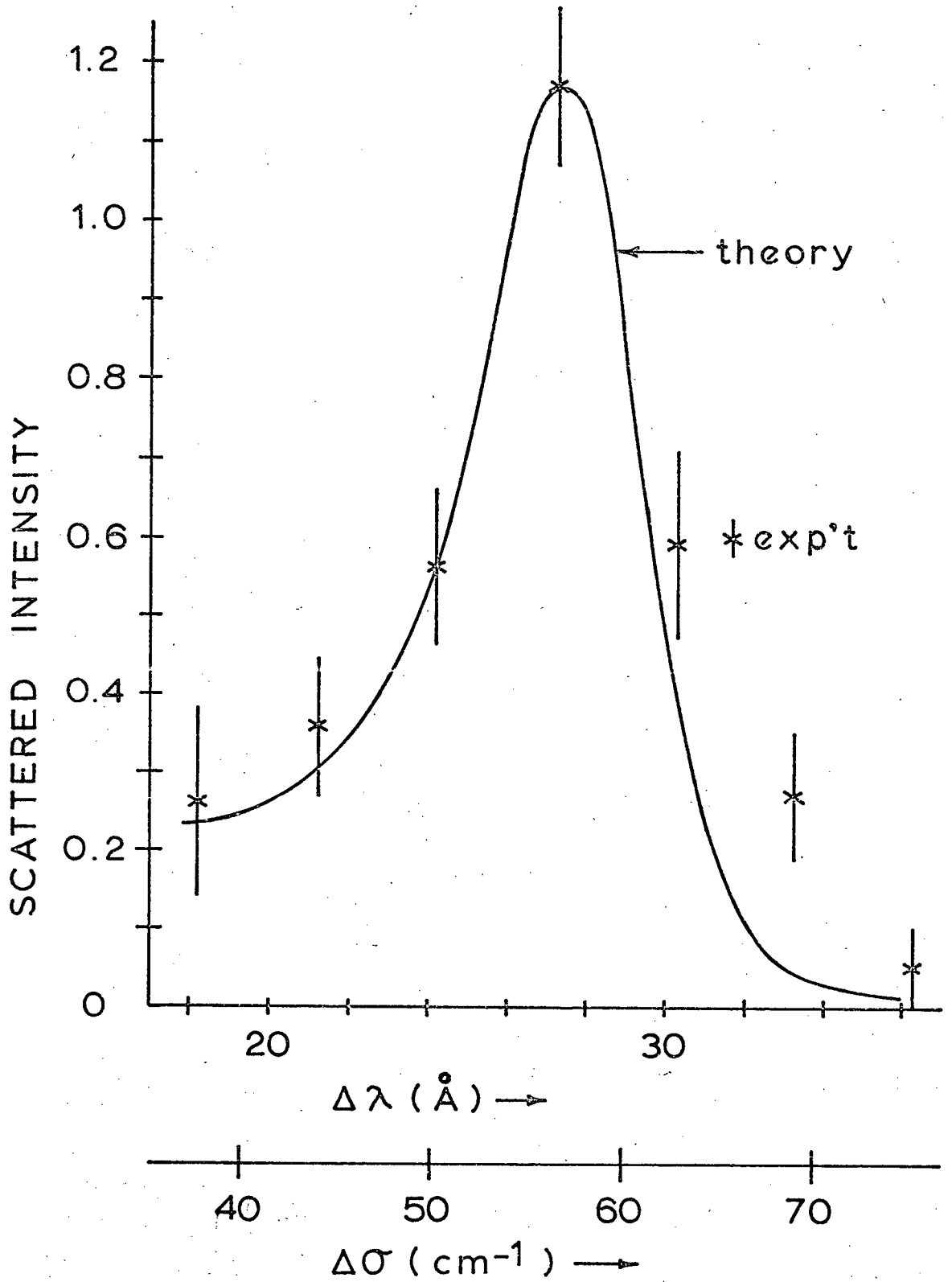

Fig. 4-3. SCATTERED LIGHT SPECTRUM NEAR THE ELECTRON SATELLITE
The curve is a theoretical profile for $n_e = 2.2 \times 10^{16} cm^{-3}$, T_e = 17,000K convoluted with the instrument profile.

(ii) ENHANCED SCATTERING

When the dye lasers were focused into the plasma, we found that the enhancement of the scattering was not great. It was thus necessary to take many shots, both with and without the dye lasers, to measure the satellite intensity as a function of the dye laser frequency difference. Since some of the components (ruby Q-switching cell windows, ruby rod surfaces and the gratings) change with time due to deterioration, it was found necessary to compare the results for a single frequency difference of the dye lasers on one day (i.e. in approximately 40 shots, which is about the lifetime of the dye). The scattered signal with and without the dye lasers focused into the plasma (normalized by the incident ruby laser power as recorded by the diode monitor) is measured for each frequency difference between the two dye lasers. The observation wavelength is kept fixed, so that $\Delta\lambda \simeq 27.2\text{Å}$ in all cases. The difference between the "with" and "without" signals is then obtained, and is converted to a relative change by dividing the change in the signal due to the dye lasers by the normal scattered signal (i.e. the "without" signal).

The results are shown in fig. 4-4. The error bars represent the standard deviation of the mean of at least

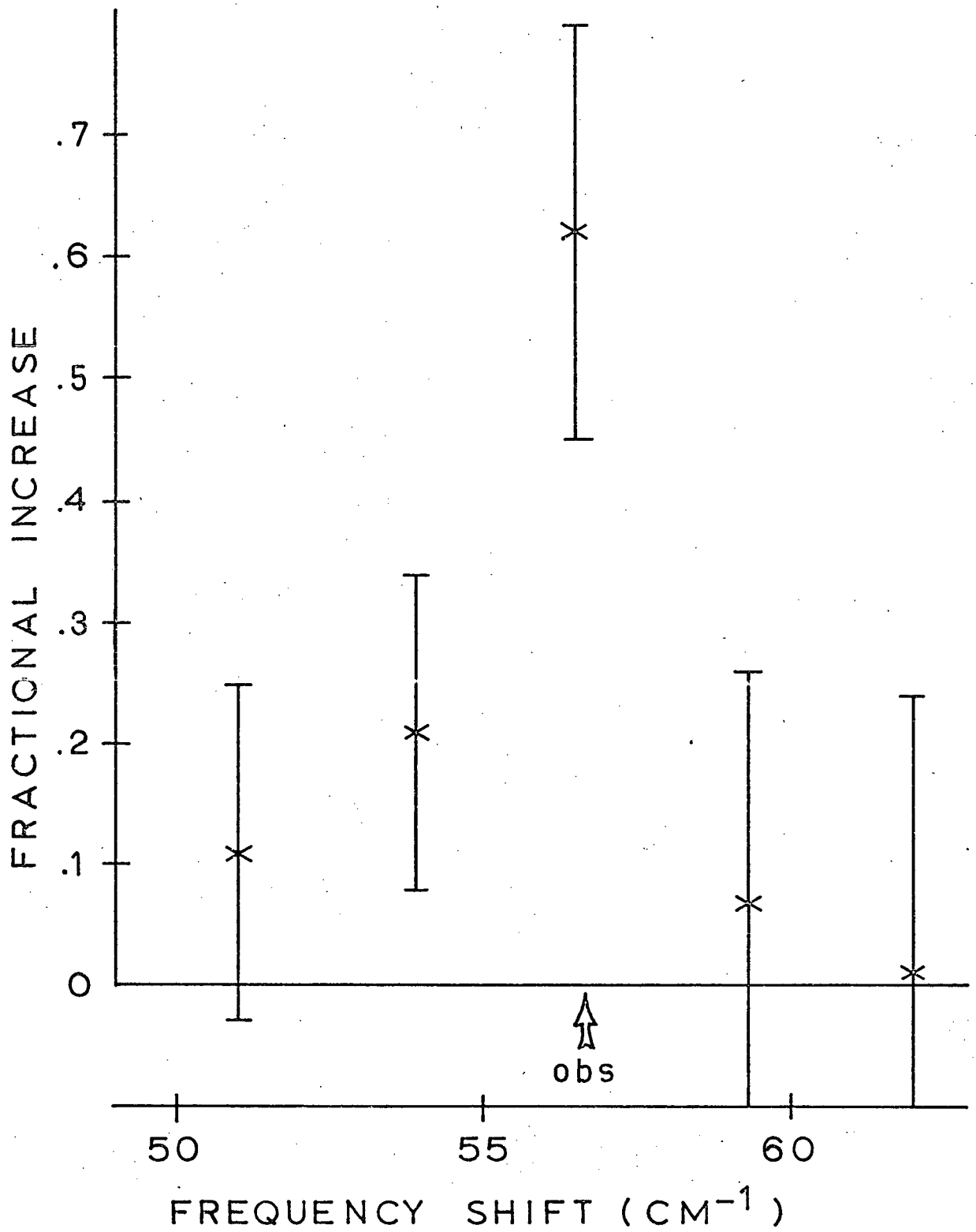

Fig. 4-4
The fractional increase of the satellite intensity as a function of the frequency difference between the dye lasers. The shift indicated by obs is that of the normally-observed satellite.

10 shots with the dye lasers and 10 shots without, except for the points at a shift of 62 cm^{-1}, where only 5 shots with the dye laser and 4 without were taken.

We can see that there is a definite increase in the intensity of the satellite when the frequency difference between the dye lasers is approximately 56 cm^{-1}. This shift corresponds very well to the observed normal resonance which appears at a frequency shift of 56.5 cm^{-1}. There does seem to be a slight asymmetry to the small-frequency-shift side of the maximum, but any examination of this effect will have to depend on a better measurement of the dye laser linewidth. As we saw in fig. 4-1, the dye laser line is slightly asymmetric, and the effect could be to cause a slight asymmetry of the enhancement.

The amplitude of the increase in the scattering signal is consistent with the wave-mixing analysis. The sample calculation in Chapter II indicates that mixing beams of 1 MW focused to a 300μ spot (with a resulting electric field of about 10^3 esu/cm) should produce a scattering

$$\frac{P_s}{P_i} \simeq 5 \times 10^{-14} \quad .$$

This is approximately the same as the scattering due to thermal fluctuations, and indeed we observe an enhancement comparable to the original satellite intensity.

CHAPTER V

CONCLUSIONS AND DISCUSSION

The scattering of ruby laser light from a Helium plasma has been observed, and the spectrum shows a distinct electron satellite at a wavelength shift of 27.2Å. The position and the shape of the satellite are reasonably consistent with an electron density of 2.2×10^{16} cm^{-3} and a temperature of 17,000 K.

We have also observed the enhancement of the high-frequency satellite when two dye lasers are focused into the scattering volume. The two lasers are derived from a common dye cell, and can produce a 1-2 MW pulse. When the frequency difference between the two dye lasers is equal to the resonant frequency of the plasma, as observed via the normal scattering technique. the intensity of the satellite is increased by about 60%. The reason for this increase cannot be any heating effect because of its resonant nature, and is clearly due to the mixing of the two dye laser beams in the plasma, driving a density fluctuation which then increases the scattering cross-section. The magnitude of the increase is consistent with theoretical calculations of wave-mixing in a plasma.

Since this investigation represents the first experimental evidence for wave-mixing of optical beams in a plasma, a discussion of the possibilities for new work would seem to be in order.

As far as this particular experiment is concerned, one must take some obvious steps to improvement:

(1) Increase the reliability of the dye laser, and increase the power output while reducing the linewidth. Dye laser amplifiers would seem to be a solution to the power problem, and there are techniques which should greatly narrow the linewidth and improve the tunability. A linewidth of .01Å has been achieved by Bradley et. al. (1968) who used a tilted Fabry-Perot interferometer, and also by Walther and Hall (1970), who employed an electrically-tuned birefringent KDP crystal.

(2) Change the mixing angle such that it is possible to pass into the collision-dominated regime, and hence determine the electron-neutral collision frequency.

If these improvements are possible, it is then hopeful that several interesting experiments can be performed. It would greatly simplify the focusing problems if one could observe the satellite features of forbidden lines as seen by Ringler and Cooper (1969). This technique would eliminate the need for the third beam and allow observation in a convenient region of the specturm.

If the amplitude of the fluctuation becomes reasonably large, we can move to a regime of nonlinear Landau damping and hence study this phenomenon with unequalled precision. Also, there will be increasingly more energy pumped into the plasma by turbulent heating from the decay of the plasma wave. This could prove to be a very useful technique for plasma heating.

Finally, a more thorough examination of the possibilities of the method as a plasma probe is necessary. It may well be that wave-mixing could complement normal laser scattering as a diagnostic technique.

BIBLIOGRAPHY

Arcese, A. (1964), Applied Optics 3, 435.

Bekefi, G. (1966), Radiation Processes in Plasmas, John Wiley.

Berk, H.L. (1964), Phys. Fluids 7, 917.

Bloembergen, N. (1967), Am. J. Phys. 35, 989.

Bradley, D.J., Durrant, A.J.F., Gale, G.M., Moore, M. and Smith, P.P. (1968), IEEE J. Quantum Electron, QE-4, 707.

Bradley, D.J., Magyar, G. and Richardson, M.C. (1965), VIIth International Conference on Phenomena in Ionized Gases.

Brown, S.C. (1959), Basic Data of Plasma Physics, M.I.T. Press.

Chan, P.W. (1966), Ph.D. Thesis, University of British Columbia.

Chan, P.W. and Nodwell, R.A. (1966), Phys. Rev. Letters 16, 122.

Churchland, M.T. (1969), M.Sc. Thesis, University of British Columbia.

Daughney, C.C., Holmes, L.S. and Paul, J. W.M. (1970), Phys. Rev. Letters 25, 497.

Evans, D.E. and Katzenstein, J. (1969), Repts. Prog. Phys. 32, 207.

Kalman, G. and Feix, M. (1969), Non-linear Effects in Plasmas - Proceedings of the 2nd Orsay Summer Institute, Gordon and Breach.

Kroll, N.M., Ron, A. and Rostoker, N. (1964), Phys. Rev. Letters 13, 83.

Maier, M., Kaiser, W. and Giordmaine, J.A. (1969), Phys. Rev. 177, 580.

Minck, R.W., Terhune, R.W. and Rado, W.G. (1963), App. Phys. Letters 3, 181.

Montgomery, D. (1965), Physica 31, 693.

Morris, R.N. (1968), M.Sc. Thesis, University of British Columbia.

Perkins, F.W. and Salpeter, E.E. (1965), Phys. Rev. 139, A55.

Perkins, F.W., Salpeter, E.E. and Yngvesson, K.O. (1965), Phys. Rev. Letters 14, 579.

Ringler, H. and Cooper, W.S. (1969), Phys. Rev. 179, 226.

Sagdeev, R.Z. and Galeev, A.A. (1969), Non-linear Plasma Theory, Benjamin.

Shkarofsky, I. (1966), A.R.L. Report 66-0234, Office of Aerospace Research W.P.A.F.B. (Dayton).

Shkarofsky, I. (1968), Plasma Phys. 10, 169.

Soffer, B.H. and McFarland, B.B. (1967), App. Phys. Letters 10, 266.

Sorokin, P.P. and Lankard, J.R. (1966), I.B.M. J. Res. Dev. 10, 162.

Spitzer, L. (1962), Physics of Fully Ionized Gases, Interscience.

Tsytovich, V.N. (1970), Non-Linear Effects in Plasma, Plenum Press.

Van der Kamp, G.S.J.P. (1968), M.Sc. Thesis, University of British Columbia.

Walther, H. and Hall, J.L. (1970), App. Phys. Letters 17, 239.

Weinstock, J. (1967), Phys. Fluids 10, 2065.

Weyl, G. (1970), Phys. Fluids 13, 1802.

Woodbury, E.J. and Ng, W.K. (1962), Proc. I.R.E. 50, 2347.

Zel'dovich, Va. B. and Raizer, Yu.P. (1966), Physics of Shock Waves and High Temperature Hydrodynamic Phenomena, Vol. 1, Academic Press.

APPENDIX A

LASERS BASED ON STIMULATED RAMAN SCATTERING

The proposal by Kroll, Ron and Rostoker (1964) that non-linear mixing of electromagnetic waves in a plasma could be observable is strongly dependent on the availability of powerful laser sources which can be tuned to the plasma resonance. When we began this experiment, dye lasers were not available; the first report on the dye laser was that of Sorokin et. al. (March 1966), and the knowledge that the line could be narrowed and tuned by a grating was not available until the work of Soffer and McFarland (May 1967). Instead, we proposed using Raman lasers, pumped by the same ruby laser, as our sources and to tune the plasma to the obtained frequency difference Δw. The use of a common pump would be the method of overcoming timing problems.

The Raman effect is an inelastic scattering of light, in which the atom or molecule extracts a specified energy from the beam (producing longer-wavelength Stokes radiation), or contributing this energy to the beam (producing shorter-wavelength anti-Stokes radiation). The processes are shown in fig. A-1. ν_p is the frequency of

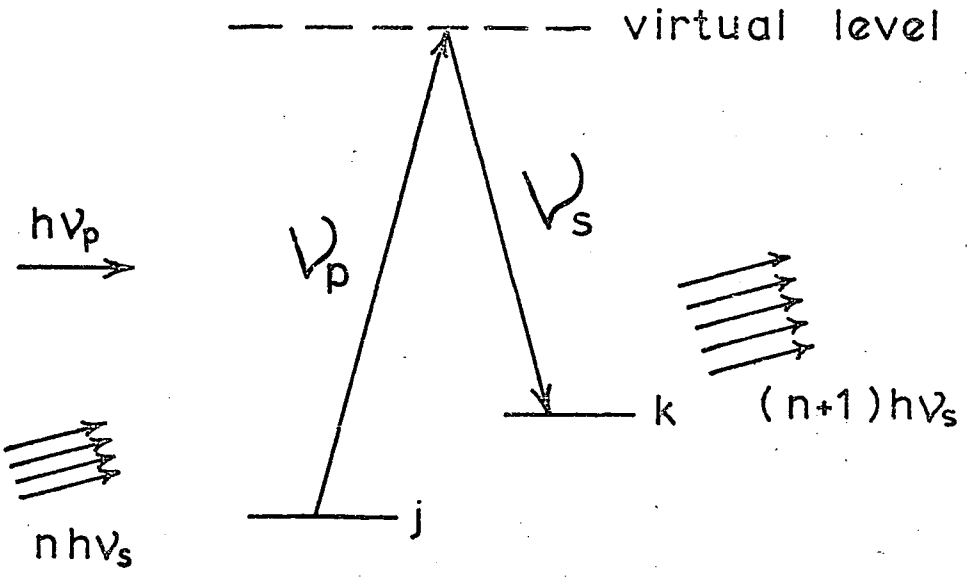

Stimulated generation of
Raman Stokes radiation

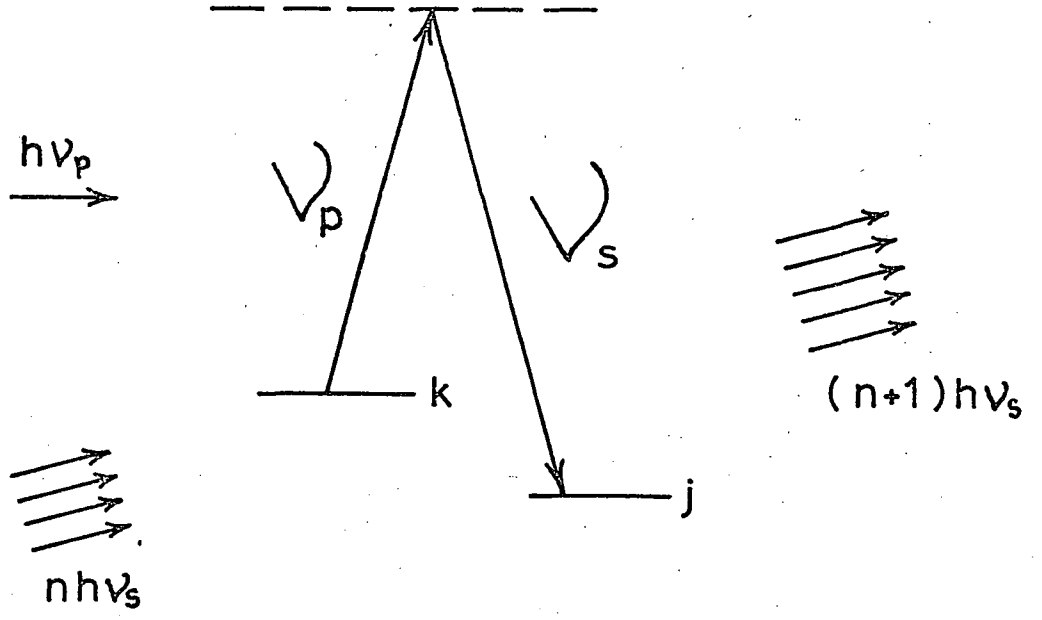

Stimulated generation of
Raman anti-Stokes radiation
fig. A-1

the incident or pumping radiation, and ν_s is the frequency of the scattered radiation. The atom or molecule changes its internal energy during the process, and the scattered photon has thus a different frequency by just this amount:

$$h\nu_s = h\nu_p \pm h\nu_{jk} \quad ,$$

where ν_{jk} is the frequency corresponding, in most cases, to the vibration frequency of the molecule. In general, the Stokes radiation is stronger than the anti-Stokes since there are more molecules in the ground state than in excited states.

The stimulated Raman effect was discovered by Woodbury and Ng (1962), and from the work of Minck et. al. (1963) it was known that a significant portion ($\simeq$ 25% in H_2) of the incident energy could be converted to 1st order Stokes radiation (radiation is also produced in other (multiple) orders but this was generally much smaller).

Since there are no materials which produce a shift close to the plasma resonance ($\Delta\sigma \simeq$ 100-120 cm^{-1} in Ar , or $\Delta\sigma \simeq$ 60 cm^{-1} in He), we were thus forced to employ 2 Raman-active materials. Thus we began a search for two compatible Raman liquids, whose vibrational frequencies differed by $\simeq$ 100 cm^{-1}. The first effort was to identify

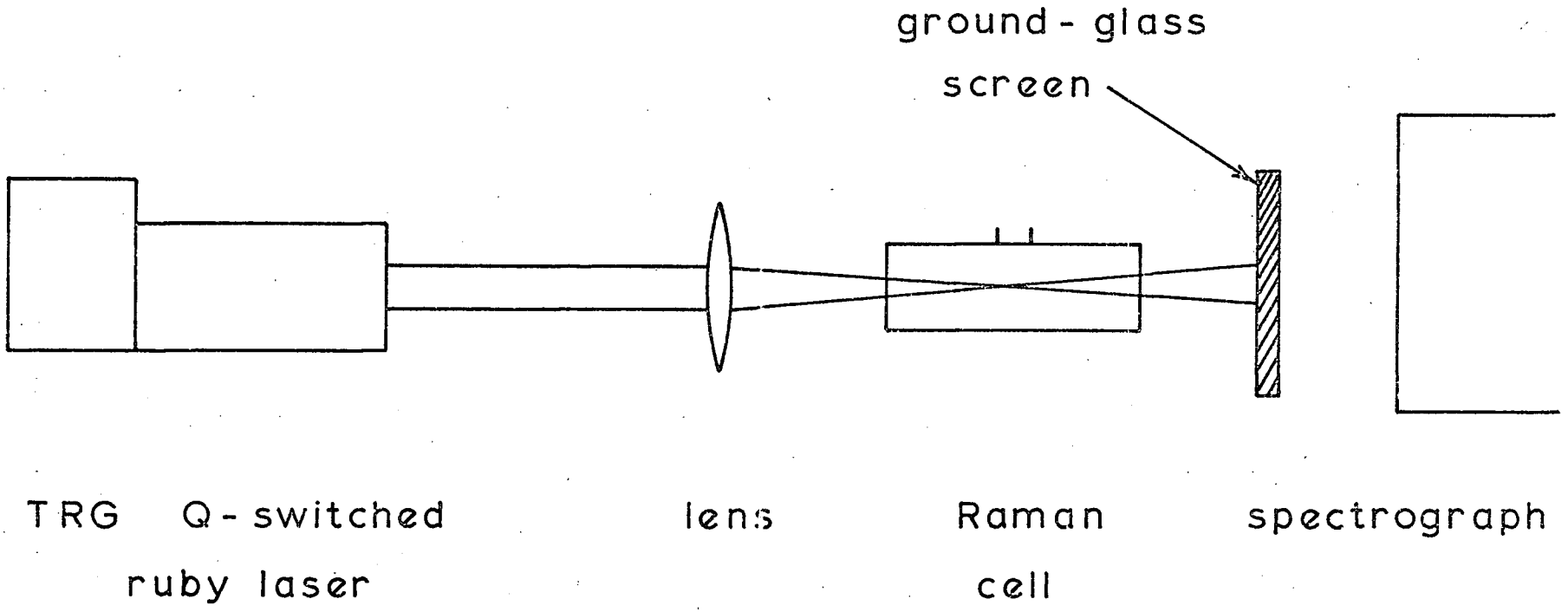

Fig. A-2

EXPERIMENTAL INVESTIGATION OF STIMULATED RAMAN SPECTRA

those materials which would lase with reasonable intensity, and to accurately measure the Raman shifts. The experimental approach is shown in fig. A-2, and the list of materials, their Raman shifts and comments is shown in table A-1.

The two materials with which I did the most work are cyclohexane and 1,2-dichloroethane, which produce Raman shifts of 2853 cm^{-1} and 2961 cm^{-1} respectively, and hence a difference of 108 cm^{-1}.

The energy output from the Raman laser was less than 1% of the input ruby energy, but there were hopes that with a more powerful laser this would be sufficient.

At this point I should note a qualitative observation: cyclohexane and dichloroethane behave quite differently as far as stimulated Raman emission is concerned. With cyclohexane lasing can rarely be achieved without using a lens in front of the cell, while dichloroethane will readily lase without a lens. From the work of many people (see the review article by Bloembergen (1967)) it was realized that the self-focusing property of the material plays a large role in achieving threshold for Stimulated Raman scattering. Cyclohexane is a rather poor self-focusing liquid, and so a lens is generally required. Dichloroethane, however, is a fairly good self-focusing material, and can concentrate the incident light to a group of small

TABLE A-1

List of Raman-active Liquids Studied

MATERIAL	RAMAN SHIFT	COMMENTS
Acetone	2923 cm	Medium intensity
Carbon disulphide	656	very strong
Carbon tetrachloride	455	strong
Cyclohexane	2853	fairly strong
	802	medium
Dichloroethane	2961	fairly strong
		reported 2956
Dichloromethane	2987	medium
		reported 2902
Ethylene chlorohydrin	2961	medium
		reported 3022
Nitrobenzene	1345	strong
Tetrahydrofuran	917 2818 2879 2965	very weak

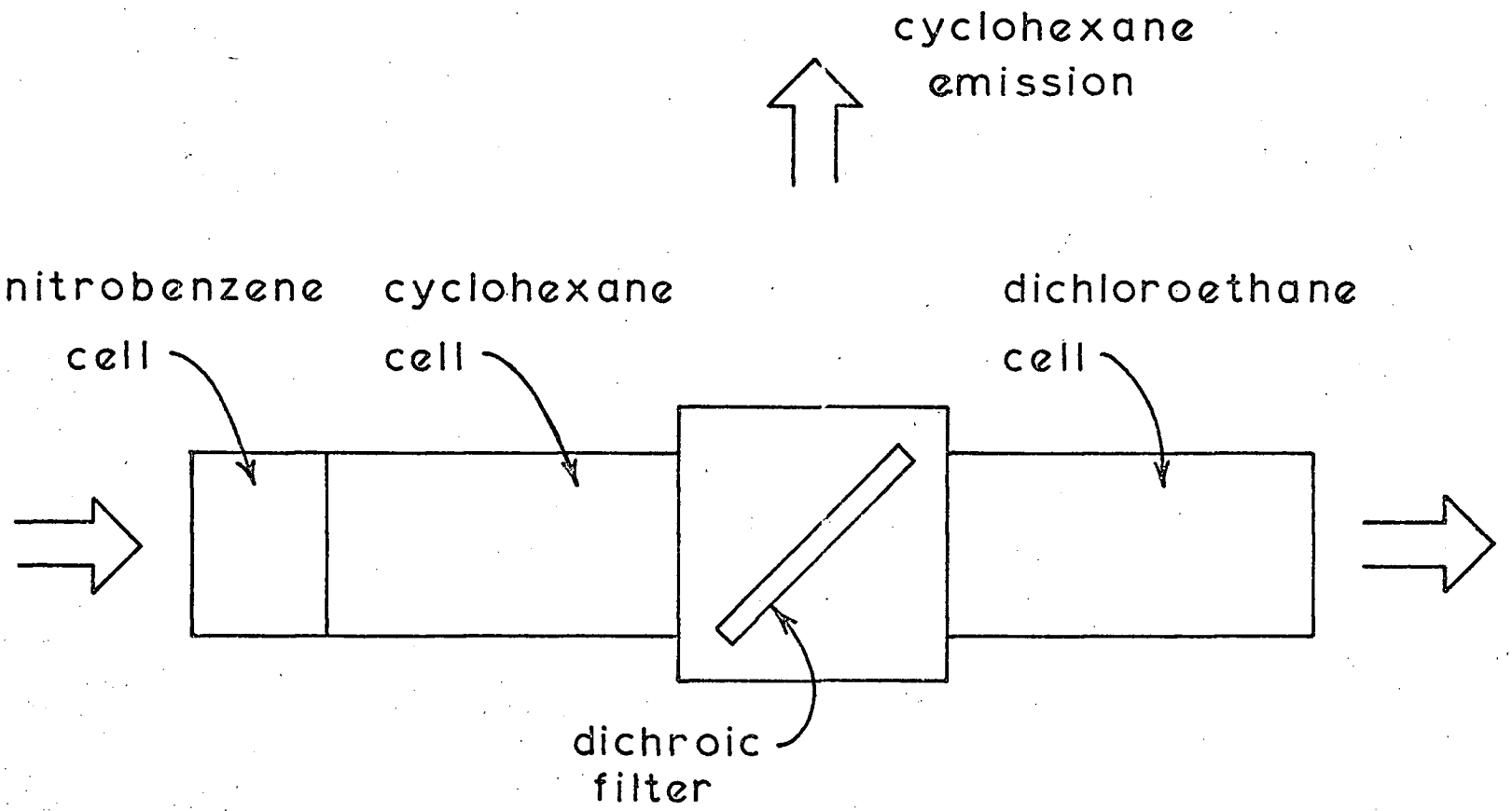

Fig. A-3
EXPERIMENT DESIGNED FOR EMISSION FROM 2 LIQUIDS

filaments without the aid of a lens. This effect then supplied us with another method of achieving Stimulated Raman Scattering in cyclohexane: place a self-focusing cell in front of it.

Thus a short cell of a very good self-focusing liquid, nitrobenzene, was placed in front of the cyclohexane cell. The use of this extra cell enabled Raman generation without using lenses, and hence the beam optics could be much simpler. The design of the Raman cells took on the shape shown in fig. A-3, being made in the form of one big cell, with 1 entrance and 1 exit interface. This configuration considerably reduces the reflection losses, and was found to be very important in observing stimulated emission from the second cell. With this scheme it was found that Raman emission could be generated from both liquids. To determine the time-behaviour of the emission, high speed oscillagrams were taken of the light output, using fast Hewlett-Packard PIN photodiodes and a Tektronix 519 oscilloscope. Some results are shown in figure A-4. Although the results can best be described as erratic, there are basic features which appear, depending on the experimental conditions. If no lens is used, or if a long focal-length lens is placed near the front of the cell, the output consists of single pulses, or short bursts of quite widely-spaced pulses. The duration of each pulse is very short, and

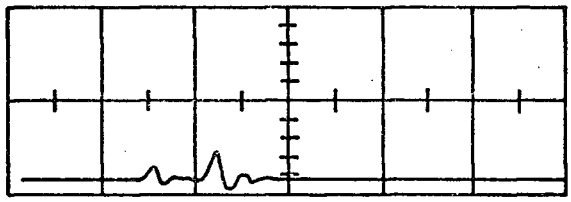

no lens

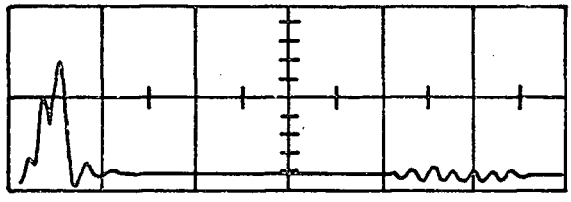

lens 2cm from
front of cell

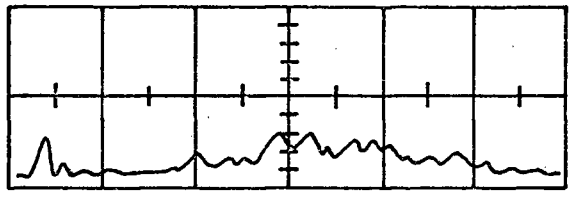

lens 4cm from
front of cell

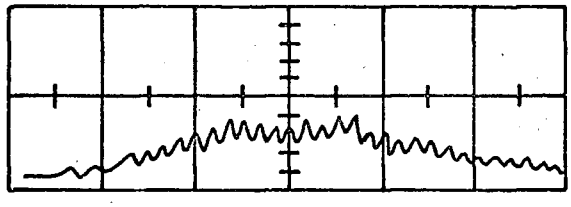

lens 6cm from
front of cell

SWEEP 5 nanosec. FOR ALL TRACES

Fig. A-4

TIME BEHAVIOUR OF RAMAN LASER EMISSION

is probably less than the 1 nanosec. risetime of the detection system. As the lens is moved farther away, so that it focuses inside the cell, there is a transition to a highly modulated pulse lasting for an appreciable time (approximately 1/3 of the pumping pulse). The nature of this modulation is not well understood, but the sharp bursts seem to be consistent with self-focusing near the rear (exit) window of the cell, and the subsequent build-up of backward, then forward, Raman emission. In fact, the oscillogram shown in fig. A-4 (a) is very similar to those seen by Maier, Kaiser and Giordmaine (1969), and the time between the pulses ($\simeq$ 3.7 nsec.) is close to the double transit time of the entire cell.

In conclusion, one could say that the erratic nature of the stimulated Raman emission indicates that rather complex processes are involved, and that self-focusing plays a dominant role in liquids. Compressed gases would seem to offer the best possibilities for the construction of a Raman laser, but the erratic nature of the emission would tend to rule out Raman lasers as a tool in wave-mixing experiments, where exact timing is essential. The dye would seem to be a better choice in almost every way.

APPENDIX B

DAMPING PROCESSES WHICH LIMIT RESONANCE

Whenever there is a forced oscillation, one finds that the maximum amplitude is determined by damping. When the driven medium is a plasma, the damping will be due to the energy and momentum lost by the particles comprising the wave through Landau damping or collisional damping of some kind.

Let us consider the possible mechanisms as they would apply to the plasma jet used in this experiment, and in particular let's calculate, for various scattering angles, the relative importance of the following:

(1) LANDAU DAMPING

Following Bekefi (1966) p. 121, we see that for a longitudinal wave to be a normal mode of oscillation of the plasma, the frequence must be complex for real k:

$$w \rightarrow w(1+i\delta) \ .$$

The damping frequency is thus:

$$\nu_L \equiv w\delta \simeq w_p \left(1 + \frac{3}{\alpha^2}\right)^{\frac{1}{2}} \sqrt{\frac{\pi}{8}}\, \alpha^3 e^{-\alpha^2/2}\, e^{-3/2}$$

where w_p is the plasma frequency

and $$\alpha = \frac{1}{\Delta k L_D}$$

is the correlation parameter.

(2) MULTIPLE (FOKKER-PLANCK) COLLISIONS

If a particle has initially a velocity υ, then via collisions it will be deflected from its original path. One can define (see Spitzer (1962) p. 121) the deflection time for multiple collisions by:

$$t_D = \frac{\upsilon^2}{(\Delta\upsilon_\perp)^2} \quad , \quad \text{where} \quad (\Delta\upsilon_\perp)^2$$

is the average rate of diffusion in the plane perpendicular to υ. We can then define the associated "deflection frequency":

$$\nu_D = \frac{1}{t_D} \simeq \frac{A_D}{v^3} \left[\phi(x) - G(x)\right]$$

where $$x = v\sqrt{\frac{m}{2kT}},$$

$$A_D = 1.61 \times 10^{18} n_e \ln \Lambda$$

T is the temperature, m is the mass and n_e the number density of the field particles.

ϕ and G are simple functions, but for a fast electron moving in a field of ions $\phi - G \simeq 1$.

Λ is the ratio of the Debye length to the average impact parameter for a 90° deflection.

(3) CLOSE, BINARY COULOMB COLLISIONS

For a binary collision in which the interaction forces are electrostatic, the impact parameter which produces a 90° deflection is (see Spitzer (1962) p. 122):

$$p_{90} = \frac{e^2}{mv^2}$$

The related collision frequency is then:

$$\nu_{90} = \upsilon\, n_e\, \pi p_0^2$$

$$= \frac{\pi n_e e^4}{m^2\, \upsilon^3}$$

where n_e is the number density of the field particles.

(4) ELECTRON-NEUTRAL ELASTIC SCATTERING

The rate of electron-neutral scattering can be expressed in terms of a probability of collision P_c, which is determined experimentally. The collision frequency is then (see Brown (1959)):

$$\nu_{en} = p_o\, P_c\, \upsilon$$

where P_o is a normalized concentration in terms of which P_c is determined. The standard density is 5.64×10^{16} atoms per cm^3, so we write $p_o = \frac{n_f}{5.64 \times 10^{16}}$, where n_f is the number density of the atoms.

In a plasma, however, the neutral particle density is not easily measured. If the plasma is in Local Thermodynamic Equilibrium, knowledge of the electron density the temperature and the pressure allow a calculation of n_f. There are suggestions (see Morris (1968)) that the electron

and ion temperatures in the Helium jet are markedly different. All indications are that $T_e \cong 18{,}000K$, while it is estimated that $T_i \simeq 5700$ K. This large difference in temperature affects greatly the neutral density.

The total pressure $P = n_e kT_e + n_i kT_i + n_f kT_f = 1.01 \times 10^6$ dynes/cm^2 (1 atmosphere).

$$n_i = n_e \simeq 2.2 \times 10^{16} \text{ cm}^{-3}$$

$$T_e \simeq 18{,}000 \text{ K}$$

$$T_i = T_f \simeq 5{,}700 \text{ K}$$

Hence by assuming charge neutrality ($n_i = n_e$) and $T_i = T_f$, we can solve for n_f:

$$n_f \simeq 1.20 \times 10^{18} \text{ cm}^{-3} .$$

This value is much larger than the neutral density calculated assuming LTE at 17,000K, which gives 3.88×10^{17} cm^{-3}.

Using these expressions as estimates of the various damping processes, it is found that close, binary coulomb collision rate is negligible compared to the others. The

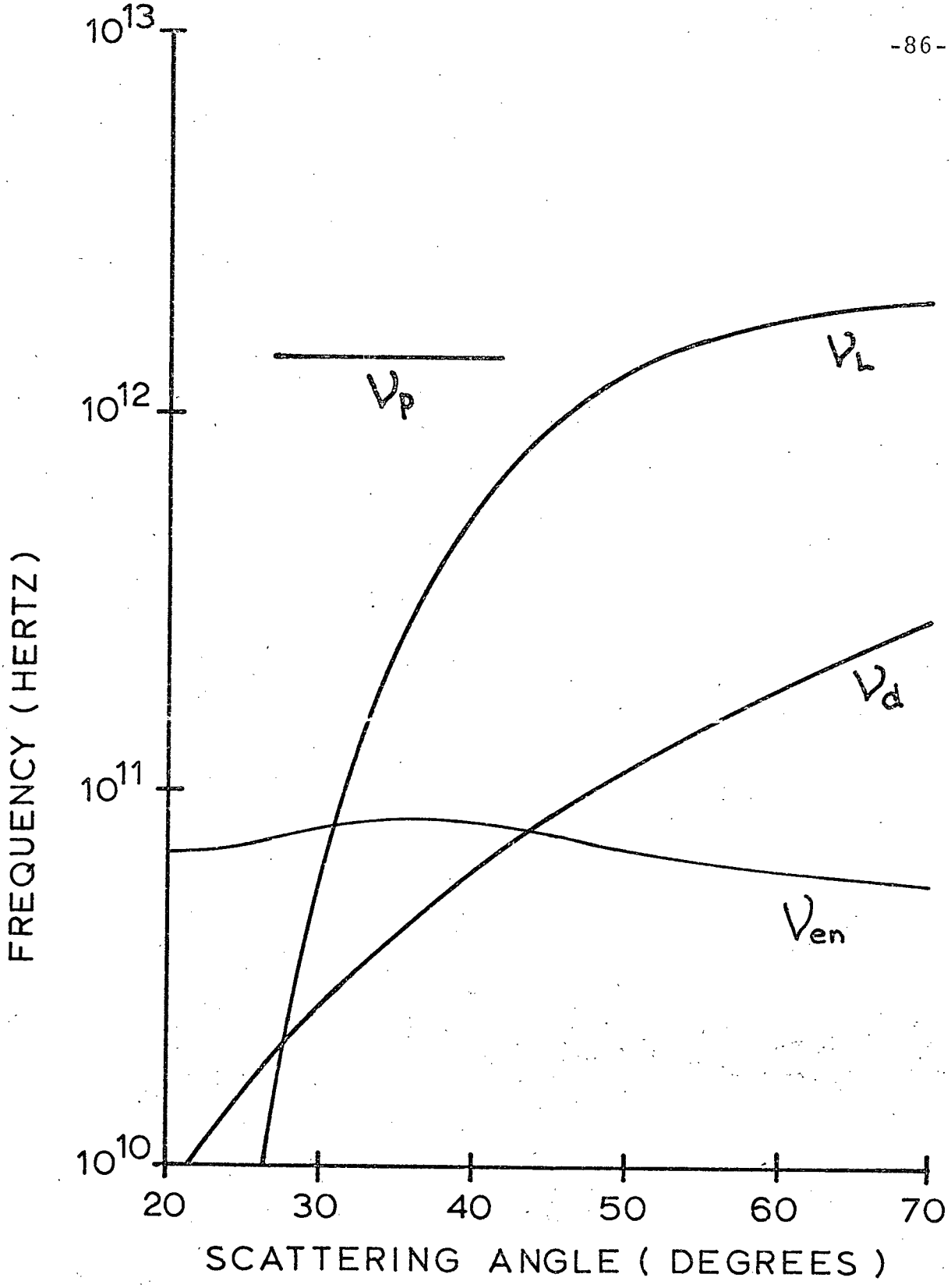

Fig. B-1

DAMPING FREQUENCIES IN HELIUM PLASMA JET

damping frequencies ν_L, ν_d and ν_{en} have been calculated as a function of scattering angle in the plasma jet, and are shown in fig. B-1. As the angle is increased, the damping becomes more severe, but over most of the range Landau damping is dominant. In the forward direction, however, electron-neutral collisions are the primary damping mechanism.

APPENDIX C

RAW DATA, CALCULATION OF THE MEANS AND STANDARD DEVIATIONS

In order to determine the effect of the dye lasers on the scattered intensity, the scattered signal (normalized by the incident ruby laser power) is measured both with the dye lasers (denote by W), and without them (denote by WO). A number of shots is taken for each setting of the frequency difference between the dye lasers.

The mean values of the scattered intensity (denoted by <W> and <WO>) are then calculated. For each value of the frequency separation $\Delta\sigma$ we can then calculate the fractional increase in the scattered intensity due to the presence of the dye laser beams:

$$Q = \frac{\langle W \rangle - \langle WO \rangle}{\langle WO \rangle} \quad .$$

Regarding Q as a function of both <W> and <WO>, the standard deviation of the mean of Q can be calculated from the standard deviations σ_W and σ_{WO}:

$$\sigma_Q^2 = \left[\frac{\partial Q}{\partial \langle W \rangle}\right]^2 \sigma_W^2 + \left[\frac{\partial Q}{\partial \langle WO \rangle}\right]^2 \sigma_{WO}^2 \quad ,$$

where:

$$\frac{\partial Q}{\partial \langle WO \rangle} = \frac{1}{\langle WO \rangle} \quad ,$$

and

$$\frac{\partial Q}{\partial \langle WO \rangle} = \frac{-\langle W \rangle}{\langle WO \rangle^2}$$

In Table C-1 are listed all the experimental results, and the calculated values for Q and σ_Q. These calculated values are the ones plotted in Fig. 4-4.

TABLE C-1

RAW DATA

$\Delta\sigma$ cm^{-1}		Values of scattered signal normalized by ruby laser power (arbitrary units)														<W> or <WO>	σ_W or σ_{WO}	Q	σ_Q
51.0	W	.84	1.10	.67	.76	.77	.65	.67								.78	.06	.11	.14
	WO	.52	.88	.82	.71	.78	.36	.85	.37	.69	1.04					.70	.07		
53.8	W	.78	.67	.42	.85	.36	.47	.67	.83	.39	.57	1.26	.71	.69	.78	.68	.06	.21	.13
	WO	.86	.50	.88	.85	.58	.64	.51	.30	.46	.29	.50	.76	.48	.41	.56	.04		
56.5	W	1.06	1.72	1.34	1.45	1.54	1.03	1.46	1.03	1.48	1.36	.89	1.65			1.33	.08	.62	.17
	WO	1.33	1.14	.94	.91	.88	.96	.58	.86	.59	.69	.65	.63	.48		.82	.07		
59.3	W	.43	.34	.43	.58	.87	1.06	.32	.72	.61	.50	.47				.58	.07	.08	.17
	WO	.48	.27	.72	.66	.50	.31	.36	1.18	.50	.33	.31	.76	.58	.62	.54	.07		
62.0	W	.55	.96	.94												.82	.13	.01	.23
	WO	.95	.64	.71	.96	.78										.81	.13		

APPENDIX D

PERTURBATION OF THE PLASMA IN THE FOCAL VOLUME BY ABSORPTION OF LASER RADIATION

When a laser beam is focused into a plasma, some of the light will be absorbed by the electrons in the focal volume. The main process of energy absorption is that of inverse bremsstrahlung. We can estimate the amount of energy absorbed in a small volume V using the absorption coefficient (Bekefi (1966), p. 87):

$$\alpha_\omega = 3.86 \times 10^{-11} \frac{n_e \; n_i}{T^{3/2} \; \omega^2} \; m^{-1} \quad ,$$

where n_e, n_i are the electron and ion densities (in m^{-3}), T is the temperature and ω the radian frequency of the radiation.

The amount of energy absorbed in a volume $V = \ell^3$ will then be $E_o \; \alpha_\omega \; \ell$, where E_o is the energy incident on the volume. If this absorbed energy all resides with the

electrons, then the change in temperature of the electrons will be:

$$\Delta(kT_e) \simeq \frac{E_o \alpha_\omega \ell}{\frac{3}{2} n_e V} = \frac{2}{3} \frac{E_o \alpha_\omega}{n_e} \frac{1}{\ell^2} \quad .$$

For lasers as used in this experiment, the minimum focal diameter will be approximately 500μ. If the incident energy is 200 mj., then the maximum change in the electron temperature, $\Delta(kT_e)$, is approximately 0.2 ev, which represents a 13% change in the temperature. If the energy absorbed by the electrons can be transferred to the ions (i.e. there is rapid electron-ion thermalization), then the absorbed energy will be shared by all the particles, and the rise in temperature of the plasma would be only:

$$\Delta(kT) \simeq 0.003 \text{ ev} \quad .$$

Thus, we might expect some change in the temperature of the plasma through absorption of radiation. The amount of additional ionization produced will be very small, however, since the ionizational potential of Helium is relatively large, and the temperature change is small.